JCI The Journal of Clinical Investigation

SUMOylation promotes extracellular vesicle-mediated transmission of lncRNA *ELNAT1* and lymph node metastasis in bladder cancer

Changhao Chen, … , Jian Huang, Tianxin Lin

J Clin Invest. 2021. https://doi.org/10.1172/JCI146431.

Research In-Press Preview Cell biology Oncology

Graphical abstract

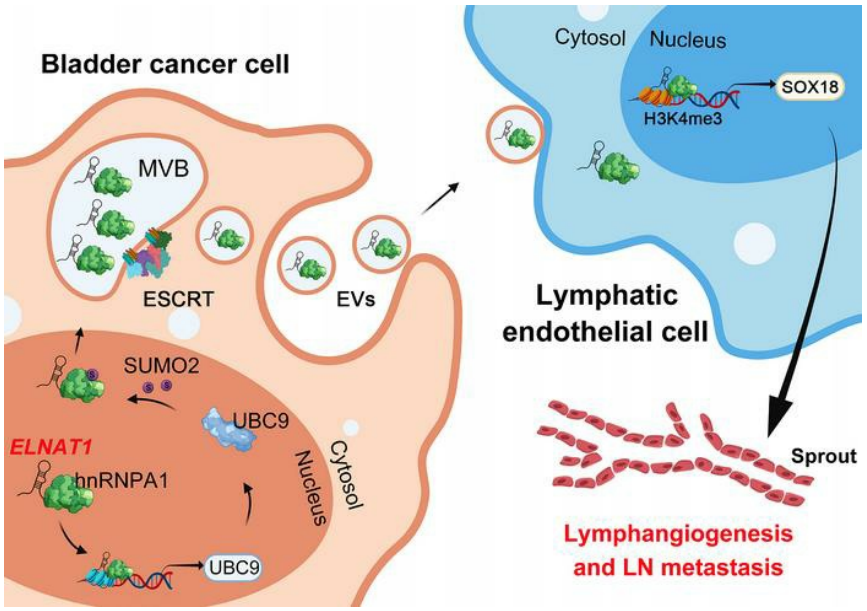

SUMOylation promotes extracellular vesicle-mediated transmission of lncRNA *ELNAT1* and lymph node metastasis in bladder cancer

Changhao Chen[1,2#*], Hanhao Zheng[1,2#], Yuming Luo[3#], Yao Kong[3], Mingjie An[1,2], Yuting Li[3], Wang He[1,2], Bowen Gao[4], Yue Zhao[5], Hao Huang[1,2], Jian Huang[1,2*], Tianxin Lin[1,2*]

[1]Department of Urology, Sun Yat-sen Memorial Hospital, Guangzhou, Guangdong, P. R. China

[2]Guangdong Provincial Key Laboratory of Malignant Tumor Epigenetics and Gene Regulation, Sun Yat-sen Memorial Hospital, State Key Laboratory of Oncology in South China, Guangzhou, Guangdong, P. R. China

[3]Department of General Surgery, Guangdong Provincial People's Hospital, Guangdong Academy of Medical Sciences, Guangzhou, Guangdong, P. R. China

[4]Department of Pancreatobiliary Surgery, Sun Yat-sen Memorial Hospital, Guangzhou, Guangdong, P. R. China

[5]Department of Tumor Intervention, Sun Yat-sen University First Affiliated Hospital, Guangzhou, Guangdong, P. R. China

* Correspondence to:
Tianxin Lin & Jian Huang & Changhao Chen. Department of Urology, Sun Yat-sen Memorial Hospital, 107 Yanjiangxi Road, Yuexiu District, Guangzhou, Guangdong Province, P. R. China, postal code: 510120; E-mail: lintx@mail.sysu.edu.cn & huangj8@mail.sysu.edu.cn & chenchh53@mail.sysu.edu.cn; Tel.: +86-13724008338, Work Tel.: +86-20-34070447; Fax: +86-20-81332336.

# These authors contributed equally to this study.

Running Title: EV-mediated *ELNAT1* promotes lymphatic metastasis of BCa

Key words: Extracellular vesicle; SUMOylation; lymph node metastasis; bladder cancer; long noncoding RNA

The authors have declared that no conflicts of interest exist.

Abstract

SUMOylation emerged as the inducer for the sorting of bioactive molecules into extracellular vesicles (EVs) triggering lymphangiogenesis, further driving tumor lymph node (LN) metastasis, but the precise mechanisms remain largely unclear. Herein, we identified that bladder cancer (BCa) cell-secreted EVs mediated the intercellular communication with human lymphatic endothelial cells (HLECs) through the transmission of a long noncoding RNA *ELNAT1*, and promoted lymphangiogenesis and LN metastasis in a SUMOylation-dependent manner in both cultured BCa cell lines and mouse models. Mechanistically, *ELNAT1* induced UBC9 overexpression to catalyze the SUMOylation of hnRNPA1 at lysine-113 residue, which mediated the recognition of *ELNAT1* by endosomal sorting complex required for transport (ESCRT) and facilitated their packaging into EVs. EV-mediated *ELNAT1* was specifically transmitted into HLECs and epigenetically activated SOX18 transcription to induce lymphangiogenesis. Importantly, blocking the SUMOylation of tumor by downregulating UBC9 expression markedly reduced lymphatic metastasis in EV-mediated *ELNAT1*-treated BCa in vivo. Clinically, EV-mediated *ELNAT1* was correlated with LN metastasis and poor prognosis of patients with BCa. These findings highlight a molecular mechanism that EV-mediated *ELNAT1*/UBC9/SOX18 regulatory axis promotes the lymphangiogenesis and LN metastasis of BCa in a SUMOylation-dependent manner, and implicate *ELNAT1* as an attractive therapeutic target for LN metastatic BCa.

Introduction

Bladder cancer (BCa) is one of the most prevalent malignancy in the genitourinary system (1). According to the infiltration of muscle, BCa develops into two distinct subtypes, 75% generating non-muscle invasive BCa (NMIBC) and 25% generating muscle invasive BCa (MIBC), among which MIBC exhibits higher risk to develop metastasis (2). Lymph node (LN) metastasis is considered as the main metastasis route and the leading cause of poor prognosis for BCa, which decreases the 5-year survival rate of patients from 77.6% to 18.6% (3). Previous study revealed that lymphangiogenesis is the pivotal and rate-limiting step in tumor LN metastasis (4), which favors tumor cells to invade the lymphatic system due to the incomplete basement membranes of neonatal lymphatic vessels (5). Despite the crucial role of lymphangiogenesis has been well-established in BCa LN metastasis, its regulatory mechanism still needs to be further elucidated.

Extracellular vesicles (EVs) are endogenous double-layered membrane vesicles that serve as molecular cargo carriers to regulate intercellular communication, resulting in LN metastasis of multiple cancers (6, 7). EVs possess highly specific fusogenic properties and uptake machinery toward recipient cells, enabling targeted regulation of tumor and tumor microenvironment (TME), which is crucial for tumor cell-TME crosstalk, leading to tumor metastasis (8, 9). Tumor cell-secreted EVs express distinct integrins that specifically target organ-specific cells and promote metastatic organotropism (10). Nonetheless, the underlying mechanism of EV-induced LN metastasis remains largely unknown and requires further investigation.

SUMOylation, a crucial post-translational modification, regulates intracellular transportation and signaling transduction by mediating protein stability and subcellular localization (11, 12). Recently, SUMOylation has been reported to play an essential role in EV packaging through mediating the recognition of molecules by endosomal sorting complex required for transport (ESCRT) and facilitating their loading into multivesicular body (MVB) (13, 14). SUMOylated hnRNPA2B1 selectively packages bioactive molecules into EVs via recognition of specific microRNAs (miRNAs) (15). SUMOylation mediates α-synuclein encapsulation into EVs with the assistance of autophagy related 5 (ATG5) (16), suggesting that SUMOylation is an important regulator for sorting molecules into EVs. However, the regulators and mechanisms triggering SUMOylation to induce EV packaging are unknown.

Long noncoding RNAs (lncRNAs), defined as a series of RNAs longer than 200-nt in length, play an important role in tumor progression (17). In the present study, we identified a lncRNA SNHG16, termed EV-mediated Lymph Node Associated Transcript 1(*ELNAT1*) which was upregulated in BCa-secreted EVs and associated positively with LN metastasis. *ELNAT1*-mediated ubiquitin carrier protein 9 (UBC9) overexpression promoted the SUMOylation of lysine-113 on hnRNPA1 ($hnRNPA1_{K113}$), thus enhancing *ELNAT1* packaging into EVs, which epigenetically activated SOX18 transcription to induce tumor lymphangiogenesis and LN metastasis. Moreover, EV-mediated *ELNAT1* showed markedly higher diagnostic efficiency for BCa LN metastasis compared with urine cytology and fluorescence in situ hybridization (FISH). These findings demonstrate a molecular mechanism that EV-mediated *ELNAT1*/UBC9/SOX18 regulatory axis promotes the

SUMOylation-dependent lymphangiogenesis and LN metastasis of BCa, indicating *ELNAT1* as a feasible therapeutic target for BCa LN metastasis.

Results

Identification of SUMOylation-associated oncogenic lncRNAs in BCa LN metastasis

Given that SUMOylation is known to play a pivotal role in initiating or sustaining tumorigenesis (18), we demonstrated that several core small ubiquitin-related modifier (SUMO) pathway components, including UBC9, SUMO2 and SUMO3, were overexpressed and correlated with poor prognosis in BCa patients (Figure 1, A-C and Supplemental Figure 1, A-D), consistently with the data from The Cancer Genome Atlas (TCGA) database (Figure 1, D-E and Supplemental Figure 1, E-H). Moreover, we found a close correlation between UBC9 and SUMO3 overexpression and LN metastasis in a 242-case cohort of patients with BCa (Figure 1F and Supplemental Figure 1I). Notably, immunohistochemistry (IHC) analysis revealed that the expression of UBC9 and SUMO3 were positively associated with microlymphatic vessel density (MLD) in the intratumor and peritumor regions (Supplemental Figure 1, J and K). As shown in Figure 1G-I and Supplemental Figure 1L-N, blocking SUMOylation by its specific inhibitor (2D-08) markedly impeded the promotion effect of BCa cells in inducing the tube formation and migration of HLECs, indicating that SUMOylation might contribute to BCa lymphangiogenesis.

We have previously demonstrated that extracellular vesicles (EVs)-mediated lncRNA transportation has been recognized as a crucial process through the signal transduction

between tumor cells and TME (19). Thus, we performed three rounds of sequencing to identify crucial SUMOylation-associated oncogenic EV-mediated lncRNAs involved in the LN metastasis of BCa. First, next-generation sequencing (NGS) was performed to determine the global expression profiles of lncRNAs in urinary EVs (urinary-EVs) of five patients with MIBC and five healthy volunteers (GEO ID: GSE156308). Supplemental Table 1 shows the characteristics of included participants. Statistical analysis revealed that 255 lncRNAs were upregulated by more than two-fold in the urinary-EVs of MIBC patients compared with that of healthy volunteers (Figure 2A). Then we intersected these lncRNAs with the results of NGS from five MIBC tissues and paired normal adjacent tissues (NATs) and in another five LN-positive paired with five LN-negative BCa tissues to further identify the EV-mediated lncRNAs required for LN metastasis of BCa (GEO ID: GSE106534). From the 255 lncRNAs validated in the first round of experiments, 12 lncRNAs that were consistently upregulated in both the urinary-EVs of MIBC patients and LN-positive BCa tissues were further selected (Figure 2B and Supplemental Table 2). Thirdly, we further detected the relationship of these 12 lncRNAs with SUMOylation to show that *ELNAT1* (SNHG16: ENSG00000163597, RefSeq accession number: NR_038108.1) dramatically promoted the expression of SUMO pathway components (Supplemental Figure 1, O and P). Using a 5' and 3' rapid amplification of cDNA ends (RACE) assay, lncRNA-*ELNAT1* was identified as a 2,538-nt intergenic transcript encoded by a gene on human chromosome 17q25.1 (Supplemental Figure 2, A-E). Analysis of TCGA database found that *ELNAT1* was consistently upregulated in tumor tissues compared with normal control and correlated positively with LN metastasis in human cancers (Supplemental Figure 3, A-G), suggesting that *ELNAT1* was a vital oncogene

involved in LN metastasis. Moreover, the higher *ELNAT1* expression was associated with poor prognosis in various cancers (Supplemental Figure 3, H-L). Therefore, we selected *ELNAT1* for further study.

ELNAT1 overexpression correlates with LN metastasis of BCa

To determine the clinical relevance of *ELNAT1* in BCa, quantitative real-time PCR (qRT-PCR) and in situ hybridization (ISH) analyses were performed to examine *ELNAT1* expression in larger clinical cohort of patients with BCa. As shown in Figure 2C-D and Supplemental Figure 4A-B, *ELNAT1* expression was dramatically higher in BCa tissues than NATs and in BCa patients with LN metastasis than those without LN metastasis. Paired metastatic LNs possessed higher *ELNAT1* expression than BCa primary tumors (Supplemental Figure 4C), implying that *ELNAT1* is a key component of LN metastatic cells. Moreover, *ELNAT1* overexpression was associated with poor prognosis of patients with BCa (Figure 2, E and F), which was consistent with the results of TCGA analysis (Supplemental Figure 4D). Notably, ISH assays indicated that *ELNAT1* expression was markedly upregulated in LN-positive BCa tissues, slightly increased in LN-negative BCa tissues, but rarely detected in NATs (Supplemental Figure 4, E and F). *ELNAT1* expression correlated positively with lymphatic vessel density in both intratumoral and peritumoral regions (Figure 2, G and H), suggesting *ELNAT1* widely involves in the lymphangiogenesis of BCa. Collectively, our results demonstrate that *ELNAT1* plays a vital role in LN metastasis of BCa.

ELNAT1 is overexpressed in BCa-secreted EVs

In light of extracellular lncRNAs mainly play crucial biological functions mediating cell-to-cell interactions and contribute to tumor LN metastasis (20), we further examined the expression of *ELNAT1* on the EVs isolated from urine samples of BCa patients and healthy participants. The results showed that *ELNAT1* was notably overexpressed in urinary EVs from BCa patients (Figure 2I). Moreover, we isolated EVs from culture medium of BCa cells. EVs with the double layer membrane structure and the size distribution of 30-150nm were characterized by transmission electron microscopy (TEM) and nanoparticle tracking analysis (NTA) (Figure 2, J and K). The EVs protein markers CD9 and ALIX were highly expressed (Figure 2L). As shown in Supplemental Figure 5A, *ELNAT1* overexpression was detected in BCa cells and their corresponding EVs compared with that in the normal bladder epithelial cells (SV-HUC-1). Moreover, *ELNAT1* expression was higher in BCa cell-secreted small EVs (characterized as about 30-150 nm in size) compared with its intracellular expression, while it was hardly detected in soluble fraction and large EVs (characterized as about 150-1000 nm in size) (Supplemental Figure 5, A-C), suggesting that *ELNAT1* may exert its function preferentially under the encapsulation by small EVs instead of large EVs or soluble fraction. Additionally, we demonstrated that *ELNAT1* expression in UM-UC-3 and T24 cell-secreted EVs was markedly upregulated by transfection with *ELNAT1* overexpressing plasmids and downregulated by knocking down *ELNAT1* in UM-UC-3 and T24 cells (Supplemental Figure 5, D-G), indicating that alteration of cellular *ELNAT1* expression impacts EV-mediated *ELNAT1* expression. Taken together, these findings demonstrate that *ELNAT1* is enriched in BCa cell-secreted EVs.

EV-mediated ELNAT1 facilitates lymphangiogenesis in vitro

Tumor-associated lymphangiogenesis, which is an independent prognostic factor in BCa, is correlated with LN metastasis (21). To evaluate whether EV-mediated *ELNAT1* promotes lymphangiogenesis in vitro, HLECs incubated with BCa cell-secreted EVs were analyzed for tube formation and migration. As shown in Supplemental Figure 5H-J, the tube formation and migration ability of HLECs was markedly enhanced when treated with EVs secreted by UM-UC-3 and T24 cells and slightly increased after incubation with EVs secreted by RT112 and UM-UC-1 cells, while no change was observed after treating with RT4 cells-secreted EVs. Moreover, *ELNAT1* knock down abolished the ability of UM-UC-3 and T24 cells-secreted EVs (UM-UC-3-$EV_{si\text{-}ELNAT1}$ or T24-$EV_{si\text{-}ELNAT1}$) to induce tube formation and migration of HLECs (Figure 3, A-C and Supplemental Figure 6, A-C). Conversely, EVs secreted by *ELNAT1*-overexpressing UM-UC-3 and T24 cells (UM-UC-3-EV_{ELNAT1} or T24-EV_{ELNAT1}) notably enhanced the tube formation and migration ability of HLECs compared with the control (Supplemental Figure 6, D-I). Taken together, these results demonstrate that EV-mediated *ELNAT1* induces lymphangiogenesis in vitro.

EV-mediated ELNAT1 promotes LN metastasis in vivo

To further investigate EV-mediated *ELNAT1* on LN metastasis in vivo, a popliteal LN metastasis model was constructed as described previously (22, 23). Mice were divided randomly into two groups (n = 12) and received injections of EVs secreted by Vector-transfected or *ELNAT1*-transfected UM-UC-3 cells (UM-UC-3-EV_{Vector} or UM-UC-3-EV_{ELNAT1}) intratumorally every three days. The tumors and popliteal LNs were

harvested when the primary tumor size reached 200 mm^3 (Figure 3D). Strikingly, UM-UC-3-EV_{ELNAT1} facilitated the metastasis of UM-UC-3 cells to popliteal LNs compared with the UM-UC-3-EV_{Vector} group, as determined by the In Vivo Imaging System (IVIS) (Figure 3, E and F). Moreover, larger popliteal LN volume and increasing LN metastatic rate were observed in the UM-UC-3-EV_{ELNAT1} group than the UM-UC-3-EV_{Vector} group (Figure 3, G-I and Supplemental Table 3). As lymphangiogenesis represents a pivotal step of LN metastasis (4), we further assessed the effect of EV-mediated *ELNAT1* on lymphangiogenesis in vivo. Importantly, UM-UC-3-EV_{ELNAT1} group dramatically increased lymphatic vessel endothelial hyaluronan receptor 1 (LYVE-1)-indicated lymphatic vessels in both intratumoral and peritumoral regions of footpad tumors (Figure 3, J and K), indicating that EV-mediated *ELNAT1* induces the lymphangiogenesis of BCa. Collectively, these results indicate that EV-mediated *ELNAT1* facilitates lymphangiogenesis and LN metastasis of BCa in vivo.

ELNAT1 directly interacts with hnRNPA1

Since the molecular functions of lncRNAs are correlated with their subcellular localization (24), FISH and subcellular fractionation assays were conducted to detect the subcellular location of *ELNAT1*, which revealed that *ELNAT1* was located in both the cytoplasm and nucleus of UM-UC-3 and T24 cells (Supplemental Figure 7, A and B). Moreover, in vitro RNA pull-down assays with biotinylated-*ELNAT1* and antisense control showed an evident band with a molecular weight ranging from 35-40 kDa (Figure 4A). HnRNPA1 was identified as the most abundant *ELNAT1*-interacting protein by mass spectrometry (MS) and western blotting analyses (Figure 4, B-D). Consistently, fluorescence staining confirmed the

co-localization of *ELNAT1* and hnRNPA1 in both UM-UC-3 and T24 cells (Figure 4E). RNA immunoprecipitation (RIP) assays demonstrated the enrichment of *ELNAT1* by endogenous hnRNPA1 (Figure 4F) further validating the interaction between *ELNAT1* and hnRNPA1. Furthermore, the sequential deletion experiments showed that the 600-750-nt region of *ELNAT1* was required for hnRNPA1 interaction (Figure 4, G and H). Sequence analysis by POSTAR2 (25) predicted a stem-loop structure in the 610-680-nt region of *ELNAT1* was potentially recognized by hnRNPA1 (Figure 4I and Supplemental Figure 7C). The deletion of 610-680-nt on *ELNAT1* impaired its enrichment by hnRNPA1 (Figure 4J), suggesting that these specific sequences are crucial to the *ELNAT1*-hnRNPA1 interaction.

ELNAT1 upregulates the SUMOylation-related E2 conjugating enzyme UBC9

To explore the molecular mechanisms underlying *ELNAT1*-induced lymphatic metastasis in BCa, we profiled *ELNAT1*-overexpressing BCa cells and control cells using NGS (Figure 5A, GEO ID: GSE156461). Since SUMOylation modification is considered to regulate the recognition of specific RNAs and participates in the process of RNAs sorting into EVs (15), we further determined the SUMOylation-associated target genes of *ELNAT1*. Among 925 genes that were regulated by *ELNAT1* ($P < 0.05$, fold changes > 1.5), we demonstrated that *UBC9* was the most markedly altered SUMOylation-related gene by qRT-PCR and western blotting analyses (Figure 5, B-D, Supplemental Figure 7D and Supplemental Table 4). To further investigate the molecular mechanisms underlying *ELNAT1* induced the transcriptional activation of UBC9 expression in BCa, luciferase assays were conducted using serial luciferase constructs containing the truncate *UBC9* promoter sequences (-2000 to +200 bp).

Our results revealed that *ELNAT1* overexpression increased the transcription activities of the -200 to +1 bp sequence in the *UBC9* promoter (Supplemental Figure 7, E and F). Then, chromatin isolation by RNA purification (ChIRP) assays showed that *ELNAT1* physiologically interacted with P1 (-153 to -143 bp) sequences in *UBC9* promoter region (Figure 5, E-F and Supplemental Figure 7G). Moreover, LongTarget, a tool for predicting lncRNA-DNA binding motifs (26), identified five potential triplex-forming oligonucleotides (TFOs) within *ELNAT1* and the paired triplex target sites (TTS) in the *UBC9* promoter. Each binding motif was subjected to circular dichroism (CD) spectroscopy and fluorescence resonance energy transfer (FRET) analysis (Supplemental Table 5). CD spectroscopy verified a notable positive peak at 270-280 nm and a negative peak at 210 nm in the *ELNAT1*/*UBC9* TTS1 group, which was similar with the FENDRR/PITX2 positive control group (Figure 5, G and H and Supplemental Figure 7H). FRET analysis revealed that the fluorescence intensity changed dramatically from 520 nm to 570-580 nm in the *ELNAT1*/*UBC9* TTS1 group compared with the control ssRNA/*UBC9* TTS1 group, which was in accordance with the FENDRR/PITX2 positive control group (Figure 5, I and J and Supplemental Figure 7I). Furthermore, we detected whether hnRNPA1 contributed to *ELNAT1*-induced transcriptional activation of UBC9 by regulating the histone methylation at the *UBC9* promoter. Chromatin immunoprecipitation (ChIP) analysis showed that overexpressing *ELNAT1* increased the enrichment of hnRNPA1 and H3K4me3 at the *UBC9* promoter, which was inhibited by deleting the *ELNAT1*-binding site of hnRNPA1 (Figure 5, K and L and Supplemental Figure 7, J and K). Meanwhile, silencing *ELNAT1* dramatically reduced the hnRNPA1 occupancy and H3K4me3 methylation at the *UBC9* promoter in UM-UC-3 and T24 cells (Figure 5, M

and N and Supplemental Figure 7, L and M), indicating that *ELNAT1* regulates the transcription of UBC9 by forming a triplex structure with its promoter sequence and inducing hnRNPA1-associated H3K4me3 modification.

UBC9-induced SUMOylation of hnRNPA1 packages ELNAT1 into EVs

It has been well-established that UBC9 could catalyze the SUMOylation of target proteins to regulate their interaction with biomolecules and cellular transportation (15, 27). The observation that *ELNAT1* directly interacted with hnRNPA1 to upregulate UBC9 expression, prompted us to hypothesize that UBC9 overexpression might stimulate the SUMOylation of hnRNPA1 to promote the packaging of *ELNAT1* into EVs. To confirm this hypothesis, co-immunoprecipitation (co-IP) assay was performed, and an obvious band ranging from 15--25 kDa was specifically enriched by hnRNPA1 (Figure 6A), which was identified as SUMO2 by MS (Supplemental Figure 8, A and B). Moreover, IP assays revealed that UBC9 overexpression enhanced the SUMO2-conjunction of hnRNPA1, suggesting that the SUMOylation of hnRNPA1 is induced by UBC9 (Figure 6B). To evaluate the specific modification sites of SUMOylation on hnRNPA1, GPS-SUMO (28), a tool for SUMOylation sites analysis, was used to obtain two potential SUMO2-conjunction residues of hnRNPA1, lysine 3 (K3) and lysine 113 (K113), which were replaced with arginine (R) (hnRNPA1$_{K3R}$, hnRNPA1$_{K113R}$) (Figure 6C and Supplemental Figure 8, C-F) and subjected to co-IP assays to show that the hnRNPA1$_{K113R}$ substitution, but not hnRNPA1$_{K3R}$, abolished the SUMOylation of hnRNPA1 (Figure 6D). Moreover, we demonstrated that *ELNAT1* overexpression upregulated the SUMOylation of hnRNPA1$_{K113}$, which was abolished by knocking down

UBC9 (Figure 6E), suggesting that *ELNAT1*-induced UBC9 overexpression promotes the SUMOylation of hnRNPA1 at K113 residue.

Next, we explored whether *ELNAT1* was packaged into BCa cell-secreted EVs by SUMOylated hnRNPA1. First, we found that *ELNAT1* exhibited a comparable EV-to-cell ratio to miR-196a and miR-320 (Figure 6F and Supplemental Figure 9A), which were previously reported to be loaded into EVs by hnRNPA1 (29, 30). HnRNPA1-silencing markedly inhibited the enrichment of *ELNAT1* in EVs secreted by BCa cells (Figure 6G and Supplemental Figure 9B), suggesting that sorting of *ELNAT1* into EVs depends on hnRNPA1. Furthermore, the truncate *ELNAT1*, which deleting the 610-680-nt sequences that containing the hnRNPA1 binding sites, was predominant retained in BCa cells rather than secreted into EVs (Figure 6H and Supplemental Figure 9C), verifying that *ELNAT1* is loaded into EVs through the interaction with hnRNPA1.

As we indicated that hnRNPA1 was SUMOylated in BCa cells, we further evaluated whether SUMOylation contributed to hnRNPA1-mediated EV-encapsulation of *ELNAT1*. SUMOylation-defective mutant of hnRNPA1 or UBC9 inhibition in BCa cells notably abolished the *ELNAT1* enrichment into *ELNAT1*-tranduced BCa-cell secreted EVs (Figure 6, I-J and Supplemental Figure 9D). $HnRNPA1_{K113R}$ transfection failed to restore the downregulation of EV-mediated *ELNAT1* after silencing hnRNPA1 as compared with $hnRNPA1_{WT}$ (Figure 6K and Supplemental Figure 9E). Importantly, confocal microscopy revealed that the accumulation of *ELNAT1* into CD63-indicated MVBs, the precursors of EVs, was downregulated markedly after UBC9 silencing or $hnRNPA1_{K113R}$ mutation (Figure 6L), indicating that the sorting of *ELNAT1* into EVs is regulated by the SUMOylation of

hnRNPA1. Additionally, we further determined whether the lysine-113 mutation of hnRNPA1 affects its interaction with *ELNAT1* thus impairing the package of *ELNAT1* into EVs. The results showed that *ELNAT1* remained directly bound to hnRNPA1 after mutating the lysine-113 on hnRNPA1 (Supplemental Figure 9, F-H), indicating that the mutation of lysine-113 on hnRNPA1 has no affection on its interaction with *ELNAT1*. Together, these results demonstrate that *ELNAT1* is packaged into BCa cell-secreted EVs by UBC9-induced SUMOylation of hnRNPA1.

EV-mediated ELNAT1 is delivered to HLECs to induce the lymphangiogenesis

As our results indicated that EV-mediated *ELNAT1* promoted lymphangiogenesis; therefore, the internalization of EV-mediated *ELNAT1* by HLECs was evaluated. Confocal microscopy revealed that punctuate fluorescent intensity was detected in HLECs incubated with PKH67-labeled EVs (Figure 7A), indicating the internalization of BCa-secreted EVs by HLECs. Moreover, incubation with UM-UC-3-EV$_{ELNAT1}$ and T24-EV$_{ELNAT1}$ markedly upregulated the *ELNAT1* expression in HLECs, while downregulating *ELNAT1* in EVs secreted by UM-UC-3 and T24 cells impaired their abilities to induced *ELNAT1* overexpression in HLECs (Figure 7, B-C and Supplemental Figure 9, I-J).

To exclude the possibility that the lymphangiogenesis were induced by activation of endogenous *ELNAT1* in HLECs, we constructed *ELNAT1* knockout HLECs (HLECs$_{ELNAT1\text{-KO}}$) (Figure 7, D and E). The effects of EV-mediated *ELNAT1* on both HLECs$_{ELNAT1\text{-WT}}$ and HLECs$_{ELNAT1\text{-KO}}$ cells were examined. Consistent with HLECs$_{ELNAT1\text{-WT}}$, the tube formation and migration ability of HLECs$_{ELNAT1\text{-KO}}$ was enhanced by EV-mediated *ELNAT1*

overexpression, while knocking down *ELNAT1* inhibited the ability of BCa cell-secreted EVs to induce the tube formation and migration of HLECs$_{ELNAT1\text{-KO}}$ (Figure 7, F-H and Supplemental Figure 10, A-I), suggesting that BCa cell-secreted EVs promotes lymphangiogenesis by transporting EV-mediated *ELNAT1* rather than transcriptionally activating endogenous *ELNAT1*. Taken together, these results demonstrate that EV-mediated *ELNAT1* is internalized by HLECs to induce BCa lymphangiogenesis.

EV-mediated ELNAT1 upregulates SOX18 expression in HLECs

Next, we analyzed the expression of lymphangiogenesis-related genes in HLECs treated with EV-mediated *ELNAT1*. Our results showed that SRY-box transcription factor 18 (*SOX18*) was the most obvious gene that positively associated with EV-mediated *ELNAT1* expression (Figure 8, A and B and Supplemental Figure 11, A and B). EV-mediated *ELNAT1* downregulation markedly decreased SOX18 expression, while overexpressing EV-mediated *ELNAT1* promoted SOX18 expression in HLECs as compared with the control (Supplemental Figure 11, C-F). It has been proposed that SOX18 represents a crucial regulator for the budding of new lymphatic vessels through the induction of genes that contributed to the phenotype of lymphatic vessels, including vascular endothelial growth factor C (VEGF-C) and prospero-related homeobox transcription factor 1 (PROX1) (31, 32). To further explore the mechanisms of EV-mediated *ELNAT1* upregulated *SOX18* expression in HLECs, a series of truncate *SOX18* promoters ranging from -2000 to +200 bp relative to the transcriptional start site were cloned into the luciferase reporter genes. As shown in Supplemental Figure 11G-H, luciferase assays revealed that EV-mediated *ELNAT1* enhanced transcriptional activity when the -800 to -400 bp region of the *SOX18* promoter was introduced in HLECs. Moreover, ChIRP assays demonstrated that EV-mediated *ELNAT1* directly interacted with

-771 to -786 bp of the *SOX18* promoter (refers to *SOX18*-P4) in HLECs (Figure 8, C and D and Supplemental Figure 11I). Mutation of the *SOX18*-P4 region reduced the luciferase activity induced by EV-mediated *ELNAT1* (Figure 8, E and F), suggesting *SOX18*-P4 was crucial for EV-mediated *ELNAT1* induced *SOX18* upregulation in HLECs. Furthermore, the enrichment of hnRNPA1 and H3K4me3 at the *SOX18* promoter was associated markedly with EV-mediated *ELNAT1* expression (Figure 8, G-J and Supplemental Figure 12, A-D), indicating that EV-mediated *ELNAT1* increases hnRNPA1-induced H3K4me3 levels at the *SOX18* promoter. Moreover, we assessed whether SOX18 was indispensable for EV-mediated *ELNAT1*-induced lymphangiogenesis. EV-mediated *ELNAT1* overexpression enhanced the tube formation and migration ability of HLECs, while downregulating SOX18 impaired EV-mediated *ELNAT1*-induced lymphangiogenesis (Figure 8, K-M and Supplemental Figure 12, E-G), indicating that SOX18 is required for EV-mediated *ELNAT1* to drive BCa lymphangiogenesis in vitro. Together, these results reveal that EV-mediated *ELNAT1* promotes BCa lymphangiogenesis via transcriptionally upregulating SOX18 expression in HLECs.

Blocking SUMOylation suppresses EV-mediated ELNAT1-induced LN metastasis

EV-mediated *ELNAT1* functions in a SUMOylation-dependent manner; therefore, we determined whether blocking UBC9-induced SUMOylation could inhibit the EV-mediated *ELNAT1*-induced lymphangiogenesis and LN metastasis of BCa. We demonstrated that *ELNAT1* overexpression notably promoted BCa cell-secreted EVs to induce lymphangiogenesis in vitro, while silencing UBC9 reversed this effect (Figure 9, A-C and Supplemental Figure 12, H-J), indicating that UBC9-induced SUMOylation contributes to the EV-mediated *ELNAT1*-induced lymphangiogenesis. Importantly, the IVIS demonstrated that

UM-UC-3-EV$_{ELNAT1}$ enhanced popliteal LN metastasis in vivo, while silencing UBC9 inhibited this effect (Figure 9, D and E). The UM-UC-3-EV$_{ELNAT1+si\text{-}UBC9\#1}$ group possessed a lower volume of popliteal LNs than the UM-UC-3-EV$_{ELNAT1}$ group (Figure 9F). Moreover, UM-UC-3-EV$_{ELNAT1}$ increased the quantification of lymphatic vessels in the footpad tumors of mice compared with the UM-UC-3-EV$_{Vector}$ group, while downregulating UBC9 expression decreased EV-mediated *ELNAT1*-induced lymphatic vessels increment (Figure 9, G and H), suggesting that blocking UBC9 impairs the effect of EV-mediated *ELNAT1* on lymphangiogenesis in vivo. Moreover, a reduction of LN metastasis rate was observed in the UM-UC-3-EV$_{ELNAT1+si\text{-}UBC9\#1}$ group as compared with the UM-UC-3-EV$_{ELNAT1}$ group (Supplemental Table 6), which was accompanied by longer survival times (Figure 9I). Taken together, these results indicate that inhibition of UBC9-induced SUMOylation suppresses EV-mediated *ELNAT1*-induced lymphangiogenesis and LN metastasis in BCa.

Clinical relevance of EV-mediated ELNAT1 in BCa patients

EV-mediated lncRNAs are regarded as promising early diagnostic biomarkers and potential therapeutic targets in BCa (33, 34). Thus, it is important to determine the clinical relevance of EV-mediated *ELNAT1* in LN metastasis of BCa. First, we found a positive correlation of the *ELNAT1* expression between urinary-EVs from BCa patients and paired BCa tissues, implying EV-mediated *ELNAT1* as an essential participant in the regulation of *ELNAT1* in BCa (Figure 10A). As we indicated that *ELNAT1* was overexpressed in LN-positive BCa, we then explored whether EV-mediated *ELNAT1* was clinically relevant to BCa LN metastasis. Strikingly, we found that urinary EV-mediated *ELNAT1* overexpression

positively correlated with LN metastasis of BCa (Figure 10B and Supplemental Figure 12K and Supplemental Table 7). Moreover, Kaplan-Meier analysis showed that BCa patients with higher EV-mediated *ELNAT1* expression were accompanied by shorter overall survival (OS) and disease-free survival (DFS) (Figure 10, C and D). Univariate and multivariate analysis revealed that EV-mediated *ELNAT1* was an independent factor for the poor prognosis of BCa patients, indicating its potential role as a therapeutic target for BCa (Supplemental Table 8 and 9). Additionally, we assessed the diagnostic performance of EV-mediated *ELNAT1* by comparing it with urine cytology and FISH, the standard non-invasive diagnostic interventions for BCa (35, 36). Receiver operating characteristic (ROC) analysis showed that urinary EV-mediated *ELNAT1* could effectively distinguish patients with BCa from healthy controls (AUC: 0.80; 95% CI: 0.76-0.80) (Figure 10E and Supplemental Table 10). Remarkably, urinary EV-mediated *ELNAT1* was highly accurate in the diagnosis of BCa LN metastasis (AUC: 0.83; 95% CI: 0.76-0.91) compared with that of urine cytology or FISH (Figure 10F and Supplemental Table 10). Furthermore, we also revealed that 63% of patients with BCa evaluated as LN-negative by computed tomography (CT) were predicted correctly as LN-positive by the detection of urinary EV-mediated *ELNAT1* (Supplemental Table 11), suggesting that urinary EV-mediated *ELNAT1* may be a better alternative to diagnose BCa LN metastasis. Consistently, higher EV-mediated *ELNAT1* expression was also observed in serum from BCa patients than heathy controls (Figure 10G). The expression of EV-mediated *ELNAT1* was upregulated in serum from BCa patients with LN metastasis than those without LN metastasis (Figure 10H). Taken together, our findings reveal that EV-mediated *ELNAT1* plays an essential role in LN-metastatic BCa (Figure 10I).

Discussion

SUMOylation mediated the sorting of RNAs into EVs to serve as an essential mediator in intercellular signal transduction, thus contributing to the crosstalk of tumor cells and the TME (37, 38). Nevertheless, the regulatory role of SUMOylation in packaging specific lncRNAs into EVs and its association with tumor LN metastasis remain largely unknown. In this study, we identified that lncRNA *ELNAT1* mediated the SUMOylation of hnRNPA1, thus regulating the sorting of *ELNAT1* into EVs and correlated with BCa LN metastasis. *ELNAT1* upregulated UBC9 expression by binding to the -153 to -143 bp region of *UBC9* promoter and recruiting hnRNPA1 to induce H3K4me3 modification, which in turn caused the SUMOylation of hnRNPA1 at K113 residue to package *ELNAT1* into EVs. Subsequently, EV-mediated *ELNAT1* directly formed a DNA-RNA triplex of *SOX18* promoter and increased hnRNPA1-induced H3K4me3 modification, transcriptionally activating *SOX18* expression and facilitating BCa LN metastasis. Our findings highlight the regulatory mechanism by which EV-mediated *ELNAT1*-induced BCa LN metastasis in a SUMOylation-dependent manner, and identify EV-mediated *ELNAT1* as a potential therapeutic target for BCa.

Lymphangiogenesis induced by SOX18 transcriptional activation has been considered as the most essential step in tumor LN metastasis (5). SOX18 is the earliest molecular hallmark of endothelial cells during embryonic development and plays an essential role in the formation of new lymphatic vessels (31, 32). Although the decisive role of SOX18 in lymphangiogenesis is well-characterized, the mechanisms of EV-mediated SOX18 expression in HLECs are unclear. Herein, we demonstrated a regulatory mechanism by which

EV-mediated *ELNAT1* activated *SOX18* transcription through directly binding to *SOX18* promoter and recruited hnRNPA1 to induce the H3K4me3 modification. Downregulating SOX18 reversed EV-mediated *ELNAT1*-induced lymphangiogenesis and LN metastasis of BCa. These findings reveal the crucial mechanism by which EV-mediated *ELNAT1* promotes LN metastasis and identify EV-mediated *ELNAT1* as a feasible therapeutic target in BCa.

SUMOylation regulates the function of proteins by influencing their subcellular localization, protein interaction, and transcriptional activity (39, 40). UBC9 is the unique E2 ligase of SUMOylation that catalyzes the conjunction of SUMOs to lysine residues of the substrates (27, 41). However, the mechanism governing UBC9-mediated SUMOylation is largely unknown. Herein, we demonstrated that EV-mediated *ELNAT1* directly formed a DNA-RNA triplex with the *UBC9* promoter to promote hnRNPA1-induced H3K4me3 modification and further induced the SUMOylation of hnRNPA1 at K113 residue. Moreover, EV-mediated *ELNAT1*-induced SUMOylation dramatically promoted the lymphangiogenesis and LN metastasis of BCa both in vitro and in vivo, suggesting that EV-mediated *ELNAT1* functions as a crucial regulator of SUMOylation-induced LN metastasis of BCa. Recently, targeting the SUMOylation pathway is considered as an effective intervention for the treatment of various cancers (42). Anacardic acid suppressed the SUMOylation pathway by targeting the SUMO-activating enzyme E1 and showed a great efficiency in the treatment of B-cell lymphoma (43). Additionally, melatonin enhanced the sensitivity of brain cells to chemotherapy through disturbing the SUMOylation-mediated nuclear translocation of Nestin (44). Therefore, the identification of the essential role of EV-mediated *ELNAT1* in the regulation of SUMOylation pathway supports EV-mediated *ELNAT1* as a potential

therapeutic target for the LN metastasis of BCa.

Urine cytology is the current standard intervention for non-invasive diagnosis of BCa, which exhibits dissatisfied sensitivity in the diagnosis of BCa (35). The appearance of FISH which possesses a higher sensitivity partly cover the deficiency of cytology but has been limited by its low specificity (45). Recently, the detection of molecules in EVs obtained from body fluid, including urine, have been widely recognized as the promising biomarkers with high efficacy for tumor diagnosis (34, 46). In the present study, we found that urinary EV-mediated *ELNAT1* possessed a slightly improvement in specificity in BCa diagnosis than FISH but has no obvious difference in sensitivity due to the higher sensitivity of FISH in the diagnosis of high grade BCa. Interestingly, the use of EV-mediated *ELNAT1* to distinguish LN-positive from LN-negative BCa obtained a satisfied sensitivity and specificity, which markedly improved the accuracy in diagnosing LN-metastatic BCa compared with FISH and urine cytology. Currently, CT and magnetic resonance imaging (MRI) are one of the most commonly recommended approach for preoperative detection of the nodal staging of BCa patients based on size and shape of LNs, which has limited accuracy in the diagnosis of microscopic metastasis (47). Herein, we found that 63% of patients with BCa evaluated as LN-negative by preoperative imaging were predicted correctly as LN-positive by the detection of urinary EV-mediated *ELNAT1*. Our findings highlight the clinical relevance of urinary EV-mediated *ELNAT1* detection in assessing LN status and support that urinary EV-mediated *ELNAT1* may represent as a better alternative to diagnose LN metastasis of BCa.

In summary, we demonstrated that EV-mediated *ELNAT1* promotds lymphangiogenesis

and LN metastasis of BCa in a SUMOylation-dependent manner. Fully elucidating the precise mechanism of EV-mediated *ELNAT1* in activating the hnRNPA1/UBC9/SOX18 axis to induce the BCa LN metastasis will not only increases our knowledge of EV-mediated LN metastasis but also enables the development of an effective therapeutic strategy for BCa.

Methods

Clinical samples

All the formalin-fixed and paraffin-embedded tissue samples were obtained from BCa patients who were pathologically confirmed as BCa by two independent pathologists and underwent surgery at Sun Yat-sen Memorial Hospital of Sun Yat-sen University. The urine samples were obtained from the same BCa patients and another 165 healthy participants. Patient information, including characteristics, clinical stage, and pathological classification, was summarized in Supplemental Table 1 and 7. Informed consent was obtained from all participants and the Ethics Committee of Sun Yat-sen Memorial Hospital of Sun Yat-sen University has approved the study mentioned above [approval number:2013(61)].

Cell lines and Cell culture

Human BCa cell lines (UM-UC-1, RT112, RT4, UM-UC-3, T24, and 5637) and human normal bladder epithelial cells (SV-HUC-1) were purchased from the American Type Culture Collection (ATCC, Manassas, VA, USA). The HLECs (Catalog 2500) were obtained from ScienCell Research Laboratories. All cell lines were cultured with 5% CO_2 at 37°C in a humidified incubator. Dulbecco's modified Eagle's medium (DMEM) (Gibco, Shanghai, China) contained with 10% fetal bovine serum (FBS) was used to culture UM-UC-3 and T24 cells, while RPMI 1640 (Gibco, Shanghai, China) were used to culture UM-UC-1, RT112 and

5637. McCoys 5A (Gibco, Shanghai, China) and F-12K medium (Hyclone, Utah, USA) both contained with 10% fetal bovine serum (FBS) were used to culture RT4 and SV-HUC-1. HLECs were cultured in endothelial cells medium (ECM) with 5% FBS (ScienCell, CA, USA).

ISH and IHC analysis

To explored the *ELNAT1* expression in formalin-fixed and paraffin-embedded tissue, *ISH* analysis was performed with the double-(5' and 3')-digoxin (DIG)-labeled *ELNAT1*-targeted probes and the scramble probe. Briefly, the slides were dewaxed with dimethylbenzene and rehydrated with gradient alcohol. Then the proteinase K was added to thoroughly digest the sections, after which the slides were hybridized with the *ELNAT1* probe at 37°C overnight. Subsequently, the slides were incubated with the anti-digoxin antibody at 37°C for 2 hours, followed with the staining using the BCIP/NBT color-substrate solution and counterstaining with nuclear fast red. The Nikon Eclipse Ti microscope (Nikon, Tokyo, Japan) was used to capture the images. The probes for ISH analysis were showed in Supplemental Table 12.

IHC analysis was conducted to further analyze the formalin-fixed and paraffin-embedded tissues obtained from the BCa patients and nude mice. All tissue sections were first processed at 60°C for 2 hours and dewaxed with dimethylbenzene, followed by the hydration with different concentrations of alcohols. Then, the antigen was repaired with EDTA and the catalase was blocked with 3% hydrogen peroxide. Subsequently, the sections were blocked with goat serum for 15 minutes, followed with the incubation of primary antibody at 4°C overnight. Finally, the sections were incubated with secondary antibodies, and the DAB and hematoxylin were used to mark the antigen and counterstain the nuclei, respectively.

The statistical significance for ISH and IHC analysis was assessed using H-score which

was calculated as followed: H-score=∑ (P × I), P: the percentage of stained cells; I: the intensity of the staining which was graded as: 0 (absent), 1 (weak), 2 (moderate) and 3 (strong).

Isolation of EVs

As for the isolation of BCa cell-secreted EVs in the cultured media, the supernatant was collected from the BCa cells which were cultured in their respective medium contained with 10% EVs-free FBS for 48h. Then, the samples were centrifuged successively 2,000g for 10 minutes, 10,000g for 30 minutes, and 120,000g for 70 minutes at 4°C to obtain EVs deposited. Subsequently, the extracted EVs in the bottom of the tube were resuspended in PBS and saved in a -80°C refrigerator for further analysis. As for the isolation of EVs from urine and serum samples, the urine and blood from all participants were collected and extracted according to the same differential centrifugation mentioned above.

All isolated EVs were further quantified by the protein content with the BCA Protein Assay Kit (Thermo Fisher Scientific, MA, USA, Cat#23227) under the instruction of manufacturers (48).

EVs internalization analysis

To verify that BCa cell-secreted EVs are internalized by HLECs, we performed the internalization experiments by labeling the isolated EVs with PKH67 green fluorescent dye. Then 10 μg/ml PKH67-labeled EVs were incubated with HLECs for 12 hours at 37°C in a humidified incubator with 5% CO_2. Subsequently, the HLECs were fixed by formaldehyde and stained with DAPI. The Zeiss confocal microscope system was used to observe the EVs internalization of HLECs and capture images.

Mouse popliteal lymphatic metastasis model

To explore the role of EV-mediated *ELNAT1* in the LN metastasis of BCa, the mouse popliteal lymphatic metastasis model was constructed with the approval of the Institutional Animal Care and Use Committee (IACUC) at Sun Yat-Sen University. Four-to-six-week-old BALB/c nude mice were acquired and kept in the animal center of Sun Yat-sen University for the duration of the experiment. Briefly, 1×10^6 UM-UC-3 cells labeled with luciferase were harvested and resuspended in PBS to be injected into the footpads of nude mice. Subsequently, the 10 μg isolated EVs from indicated BCa cells supplemented in 50 μL PBS or equivalent PBS were injected intratumorally every 3 days following the widely used protocols (49). The metastasis of popliteal LNs was monitored weekly through the IVIS until the primary tumor size reached 200 mm^3.Then, the footpad tumors and popliteal LNs of the nude mice were dissected to be further analyzed by IHC. The Nikon Eclipse Ti microscope was used to visualize the sections.

RNA pull-down analysis

The RNA pull-down assay was conducted to detect the binding proteins of *ELNAT1* in BCa cells. Firstly, the biotinylated full-length *ELNAT1* and antisense sequences were acquired through the Transcript Aid T7 High Yield Transcription Kit (Thermo Fisher Scientific, MA, USA, Cat#K0441) with the instruction of manufacturer. Then, the Pierce Magnetic RNA-Protein Pull-down Kit (Thermo Fisher Scientific, MA, USA, Cat#20164) was used to perform the pulldown assays according to the manufacturer protocols, in which the biotinylated *ELNAT1* and antisense were incubated with BCa cells lysate to pull down the

binding proteins. Finally, the binding proteins were eluted to be analyzed by silver staining or western blot, and the different band was further analyzed through a MALDI-TOF instrument (Bruker Daltonics).

ChIRP analysis

According to the protocol of Magna ChIRP RNA Interactome Kit (Millipore, MA, USA, Cat#17-10494), the ChIRP assays followed with qRT-PCR analysis were carried out to detect the interaction between *ELNAT1* and the target genes promoter. 2×10^7 BCa cells or HLECs treated with 10 μg/ml indicated EVs per group were fixed with 1% glutaraldehyde and lysed in the cell lysis buffer. Then, the cell lysate was sonicated into 100-200 bp fragments in an ultrasonic processor at 4°C for 1 hour, which further incubated with the biotinylated *ELNAT1* probes (Supplemental Table 12) at 4°C overnight. Subsequently, the pretreated beads were added to extract the DNA and analysis with qRT-PCR.

Bioinformatics analysis

The TCGA data was obtained from GEPIA (http://gepia.cancer-pku.cn/index.html). The SUMO2-conjuction site of hnRNPA1 was predicted by GPS-SUMO (http://sumosp.biocuckoo.org). The structure model of *ELNAT1* was obtained from RNAalifold (http://rna.tbi.univie.ac.at/cgi-bin/RNAWebSuite/RNAalifold.cgi). The enrichment of the binding sequences of hnRNPA1 was predicted by POSTAR2 (http://lulab.life.tsinghua.edu.cn/postar2).

Antibodies

The antibodies used in this study are as follows: anti-UBC9 (Abcam, ab75854); anti-SUMO3 (Abcam, ab203570); anti-LYVE-1 (Abcam, ab218535); anti-β-actin (Sigma-Aldrich, A5441); anti-CD9 (Cell Signaling Technology, 13403); anti-ALIX (Cell Signaling Technology, 92880); anti-hnRNPA1 (Abcam, ab5832); anti-SUMO2 (Abcam, ab233222); anti-His (Abcam, ab5000); anti-H3K4me3 (Abcam, ab1012); anti-rabbit IgG-HRP (Cell Signaling Technology, 7074); anti-SOX18 (Abcam, ab109194); anti-mouse IgG-HRP (Cell Signaling Technology, 7076); anti-rabbit IgG-HRP (Proteintech, SA00001-2); anti-mouse IgG-HRP (Proteintech, SA00001-1).

Further applied methods

Additional methods for electron microscopy analysis, lentivirus infection, cell transfection, RACE, RNA extraction, qRT-PCR analysis, western blotting analysis, FISH, immunofluorescence (IF), nuclear fractionation, tube formation assays, Transwell assays, RIP assays, serial deletion analysis, dual-luciferase reporter, FRET spectroscopy, CD spectroscopy, ChIP analysis, IP assays, co-IP assays, clustered regularly interspaced short palindromic repeats / CRISPR associated protein 9 (CRISPR/Cas9)-mediated genes deletion were further introduced in the Supplemental Methods.

Statistical analysis

All experiments in the present study were performed three separate times independently. The quantitative data were presented as the mean ± standard derivation (SD). The $\chi 2$ test was

conducted to compare the nonparametric variables. Two-tail Student's t-test or 1-way ANOVA were used for the comparison of parametric variables. The Kaplan-Meier method was carried out to assess the survival times of patients and animals. All data analysis was performed by SPSS v.13.0, and $P < 0.05$ was considered as statistically significant.

Study Approval

All the tissues or urine samples used in the present study were obtained from patients and healthy volunteers with the informed consent from all participants or their appropriate surrogates and the approval of the Ethics Committee of Sun Yat-sen Memorial Hospital of Sun Yat-sen University [approval number:2013(61)]. All the animal experiments were performed with the approval of the IACUC at Sun Yat-Sen University [approval number:2013(61)].

Author Contributions

CC and TL participated in the study design. CC, HZ, and YK performed the in vitro and in vivo experiments. YL, BG, and YZ conducted the data analyses. HH and WH performed the clinical data analyses. YL, YK, and JH performed the IF and IHC experiments. MA and YL conducted the western bolting analysis. CC, HZ, and YL wrote the manuscript. All authors have read and approved of the final manuscript. Authorship order among the co-first authors was depended on their relative contributions.

Acknowledgments

The authors thank Prof. JX Zhang of the Department of Medical Statistics and Epidemiology, Sun Yat-sen University, for statistical advice and research comments. This study was funded by the National Key Research and Development Program of China (Grant No. 2018YFA0902803, 2017YFC1308600); the National Natural Science Foundation of China (Grant No. 81825016, 81802530, 81830082, 81672395, 81871945, 81772719, 81772728, 82072639, 91740119); the Key Areas Research and Development Program of Guangdong (Grant No. 2020A1515010815, 2018B010109006, 2017A020215072); the Science and Technology Planning Project of Guangdong Province (Grant No. 202002030388, 201803010049, 2017B020227007, 201704020097); Yixian Youth project of Sun Yat-sen Memorial Hospital (Grant No. YXQH201812); Young Teacher Training Funding of Sun Yat-sen University (Grant No. 19ykpy121).

Abbreviations

EV, extracellular vesicle; LN, lymph node; BCa, bladder cancer; HLECs, human lymphatic endothelial cells; NMIBC, non-muscle invasive bladder cancer; MIBC, muscle invasive bladder cancer; TME, tumour microenvironment; ESCRT, endosomal sorting complex required for transport; MVB, multivesicular body; HnRNPs, heterogeneous nuclear ribonucleoproteins; miRNAs, microRNAs; ATG5, autophagy-related gene 5; lncRNAs, long-noncoding RNAs; *ELNAT1*, EV-mediated lymph node associated transcript 1; UBC9, ubiquitin carrier protein 9; hnRNPA1$_{K113}$, lysine-113 on hnRNPA1; FISH, fluorescence in situ hybridization; SUMO, small ubiquitin-related modifier; TCGA, The Cancer Genome Atlas; IHC, immunohistochemistry; MLD, microlymphatic vessel density; NGS, next-generation sequencing; urinary-EVs, urinary EVs; NAT, normal adjacent tissue; RACE, rapid amplification of cDNA ends; ISH, in situ hybridization; qRT-PCR, quantitative real-time PCR; TEM, transmission electron microscopy; NTA, nanoparticle tracking analysis; SV-HUC-1, human normal bladder epithelial cells; IVIS, In Vivo Imaging System; LYVE-1, lymphatic vessel endothelial hyaluronan receptor 1; MS, mass spectrometry; RIP, RNA immunoprecipitation; ChIRP, Chromatin isolation by RNA purification; TFOs, triplex-forming oligonucleotides; TTS, triplex target sites; CD, circular dichroism; FRET, fluorescence resonance energy transfer; ChIP, Chromatin immunoprecipitation; co-IP, co-immunoprecipitation; SOX18, SRY-box transcription factor 18; VEGF-C, vascular endothelial growth factor C; PROX1, prospero-related homeobox transcription factor 1; OS, overall survival; DFS, disease-free survival; ROC, receiver operating characteristic; AUC, area under the curve; CT, computed tomography; MRI, magnetic resonance imaging; ATCC, American Type Culture Collection; DMEM, Dulbecco's modified Eagle's medium; FBS, fetal

bovine serum; ECM, endothelial cells medium; IACUC, Institutional Animal Care and Use Committee; IF, Immunofluorescence; CRISPR/Cas9, clustered regularly interspaced short palindromic repeats / CRISPR associated protein 9; SD, standard deviation; ANOVA, analysis of variance.

References

1. Bray F, Ferlay J, Soerjomataram I, Siegel RL, Torre LA, and Jemal A. Global cancer statistics 2018: GLOBOCAN estimates of incidence and mortality worldwide for 36 cancers in 185 countries. *CA Cancer J Clin.* 2018;68(6):394-424.
2. Cumberbatch MGK, Jubber I, Black PC, Esperto F, Figueroa JD, Kamat AM, et al. Epidemiology of Bladder Cancer: A Systematic Review and Contemporary Update of Risk Factors in 2018. *Eur Urol.* 2018;74(6):784-95.
3. Leveridge MJ, Siemens DR, Mackillop WJ, Peng Y, Tannock IF, Berman DM, et al. Radical cystectomy and adjuvant chemotherapy for bladder cancer in the elderly: a population-based study. *Urology.* 2015;85(4):791-8.
4. Karaman S, and Detmar M. Mechanisms of lymphatic metastasis. *J Clin Invest.* 2014;124(3):922-8.
5. Escobedo N, and Oliver G. Lymphangiogenesis: Origin, Specification, and Cell Fate Determination. *Annu Rev Cell Dev Biol.* 2016;32:677-91.
6. Kalluri R. The biology and function of exosomes in cancer. *J Clin Invest.* 2016;126(4):1208-15.
7. Steinbichler TB, Dudas J, Riechelmann H, and Skvortsova, II. The role of exosomes in cancer metastasis. *Semin Cancer Biol.* 2017;44:170-81.
8. Mathieu M, Martin-Jaular L, Lavieu G, and Thery C. Specificities of secretion and uptake of exosomes and other extracellular vesicles for cell-to-cell communication. *Nat Cell Biol.* 2019;21(1):9-17.
9. Rodrigues G, Hoshino A, Kenific CM, Matei IR, Steiner L, Freitas D, et al. Tumour exosomal CEMIP protein promotes cancer cell colonization in brain metastasis. *Nat Cell Biol.* 2019;21(11):1403-12.
10. Hoshino A, Costa-Silva B, Shen TL, Rodrigues G, Hashimoto A, Tesic Mark M, et al. Tumour exosome integrins determine organotropic metastasis. *Nature.* 2015;527(7578):329-35.
11. Fu H, Liu N, Dong Q, Ma C, Yang J, Xiong J, et al. SENP6-mediated M18BP1 deSUMOylation regulates CENP-A centromeric localization. *Cell Res.* 2019;29(3):254-7.
12. Zhou L, Zheng L, Hu K, Wang X, Zhang R, Zou Y, et al. SUMOylation stabilizes hSSB1 and enhances the recruitment of NBS1 to DNA damage sites. *Signal Transduct Target Ther.* 2020;5(1):80.
13. Larios J, Mercier V, Roux A, and Gruenberg J. ALIX- and ESCRT-III-dependent sorting of tetraspanins to exosomes. *J Cell Biol.* 2020;219(3).
14. Mercier V, Larios J, Molinard G, Goujon A, Matile S, Gruenberg J, et al. Endosomal membrane tension regulates ESCRT-III-dependent intra-lumenal vesicle formation. *Nat Cell Biol.* 2020;22(8):947-59.
15. Villarroya-Beltri C, Gutierrez-Vazquez C, Sanchez-Cabo F, Perez-Hernandez D, Vazquez J, Martin-Cofreces N, et al. Sumoylated hnRNPA2B1 controls the sorting of miRNAs into exosomes through binding to specific motifs. *Nat Commun.* 2013;4:2980.
16. Kunadt M, Eckermann K, Stuendl A, Gong J, Russo B, Strauss K, et al. Extracellular vesicle sorting of alpha-Synuclein is regulated by sumoylation. *Acta Neuropathol.* 2015;129(5):695-713.
17. Flippot R, Beinse G, Boileve A, Vibert J, and Malouf GG. Long non-coding RNAs in genitourinary malignancies: a whole new world. *Nat Rev Urol.* 2019;16(8):484-504.
18. Kim JH, Choi HJ, Kim B, Kim MH, Lee JM, Kim IS, et al. Roles of sumoylation of a reptin

chromatin-remodelling complex in cancer metastasis. *Nat Cell Biol.* 2006;8(6):631-9.
19. Chen C, Luo Y, He W, Zhao Y, Kong Y, Liu H, et al. Exosomal long noncoding RNA LNMAT2 promotes lymphatic metastasis in bladder cancer. *J Clin Invest.* 2020;130(1):404-21.
20. Xie Y, Dang W, Zhang S, Yue W, Yang L, Zhai X, et al. The role of exosomal noncoding RNAs in cancer. *Mol Cancer.* 2019;18(1):37.
21. He W, Zhong GZ, Jiang N, Wang B, Fan XX, Chen CH, et al. Long noncoding RNA BLACAT2 promotes bladder cancer-associated lymphangiogenesis and lymphatic metastasis. *Journal of Clinical Investigation.* 2018;128(2):861-75.
22. Chen CH, He W, Huang J, Wang B, Li H, Cai QQ, et al. LNMAT1 promotes lymphatic metastasis of bladder cancer via CCL2 dependent macrophage recruitment. *Nat Commun.* 2018;9.
23. Kong Y, Li Y, Luo Y, Zhu J, Zheng H, Gao B, et al. circNFIB1 inhibits lymphangiogenesis and lymphatic metastasis via the miR-486-5p/PIK3R1/VEGF-C axis in pancreatic cancer. *Mol Cancer.* 2020;19(1):82.
24. Marchese FP, Raimondi I, and Huarte M. The multidimensional mechanisms of long noncoding RNA function. *Genome Biol.* 2017;18(1):206.
25. Zhu Y, Xu G, Yang YT, Xu Z, Chen X, Shi B, et al. POSTAR2: deciphering the post-transcriptional regulatory logics. *Nucleic Acids Res.* 2019;47(D1):D203-D11.
26. He S, Zhang H, Liu H, and Zhu H. LongTarget: a tool to predict lncRNA DNA-binding motifs and binding sites via Hoogsteen base-pairing analysis. *Bioinformatics.* 2015;31(2):178-86.
27. Jakobs A, Himstedt F, Funk M, Korn B, Gaestel M, and Niedenthal R. Ubc9 fusion-directed SUMOylation identifies constitutive and inducible SUMOylation. *Nucleic Acids Res.* 2007;35(17):e109.
28. Zhao Q, Xie Y, Zheng Y, Jiang S, Liu W, Mu W, et al. GPS-SUMO: a tool for the prediction of sumoylation sites and SUMO-interaction motifs. *Nucleic Acids Res.* 2014;42(Web Server issue):W325-30.
29. Qin X, Guo H, Wang X, Zhu X, Yan M, Wang X, et al. Exosomal miR-196a derived from cancer-associated fibroblasts confers cisplatin resistance in head and neck cancer through targeting CDKN1B and ING5. *Genome Biol.* 2019;20(1):12.
30. Gao X, Wan Z, Wei M, Dong Y, Zhao Y, Chen X, et al. Chronic myelogenous leukemia cells remodel the bone marrow niche via exosome-mediated transfer of miR-320. *Theranostics.* 2019;9(19):5642-56.
31. Moustaqil M, Fontaine F, Overman J, McCann A, Bailey TL, Rudolffi Soto P, et al. Homodimerization regulates an endothelial specific signature of the SOX18 transcription factor. *Nucleic Acids Res.* 2018;46(21):11381-95.
32. Francois M, Caprini A, Hosking B, Orsenigo F, Wilhelm D, Browne C, et al. Sox18 induces development of the lymphatic vasculature in mice. *Nature.* 2008;456(7222):643-7.
33. Zhan Y, Du L, Wang L, Jiang X, Zhang S, Li J, et al. Expression signatures of exosomal long non-coding RNAs in urine serve as novel non-invasive biomarkers for diagnosis and recurrence prediction of bladder cancer. *Mol Cancer.* 2018;17(1):142.
34. LeBleu VS, and Kalluri R. Exosomes as a Multicomponent Biomarker Platform in Cancer. *Trends Cancer.* 2020.
35. Talukdar S, Emdad L, Das SK, Sarkar D, and Fisher PB. Noninvasive approaches for detecting and monitoring bladder cancer. *Expert Rev Anticancer Ther.* 2015;15(3):283-94.
36. Marin-Aguilera M, Mengual L, Ribal MJ, Musquera M, Ars E, Villavicencio H, et al. Utility of

fluorescence in situ hybridization as a non-invasive technique in the diagnosis of upper urinary tract urothelial carcinoma. *Eur Urol.* 2007;51(2):409-15; discussion 15.
37. Dassler-Plenker J, Kuttner V, and Egeblad M. Communication in tiny packages: Exosomes as means of tumor-stroma communication. *Biochim Biophys Acta Rev Cancer.* 2020;1873(2):188340.
38. Chen F, Chen J, Yang L, Liu J, Zhang X, Zhang Y, et al. Extracellular vesicle-packaged HIF-1alpha-stabilizing lncRNA from tumour-associated macrophages regulates aerobic glycolysis of breast cancer cells. *Nat Cell Biol.* 2019;21(4):498-510.
39. Yu F, Shi G, Cheng S, Chen J, Wu SY, Wang Z, et al. SUMO suppresses and MYC amplifies transcription globally by regulating CDK9 sumoylation. *Cell Res.* 2018;28(6):670-85.
40. Zhao X. SUMO-Mediated Regulation of Nuclear Functions and Signaling Processes. *Mol Cell.* 2018;71(3):409-18.
41. Bossis G, and Melchior F. Regulation of SUMOylation by reversible oxidation of SUMO conjugating enzymes. *Mol Cell.* 2006;21(3):349-57.
42. Eifler K, and Vertegaal ACO. SUMOylation-Mediated Regulation of Cell Cycle Progression and Cancer. *Trends Biochem Sci.* 2015;40(12):779-93.
43. Hoellein A, Fallahi M, Schoeffmann S, Steidle S, Schaub FX, Rudelius M, et al. Myc-induced SUMOylation is a therapeutic vulnerability for B-cell lymphoma. *Blood.* 2014;124(13):2081-90.
44. Lee H, Lee HJ, Jung JH, Shin EA, and Kim SH. Melatonin disturbs SUMOylation-mediated crosstalk between c-Myc and nestin via MT1 activation and promotes the sensitivity of paclitaxel in brain cancer stem cells. *J Pineal Res.* 2018;65(2):e12496.
45. Placer J, Espinet B, Salido M, Sole F, and Gelabert-Mas A. Clinical utility of a multiprobe FISH assay in voided urine specimens for the detection of bladder cancer and its recurrences, compared with urinary cytology. *Eur Urol.* 2002;42(6):547-52.
46. Zhou B, Xu K, Zheng X, Chen T, Wang J, Song Y, et al. Application of exosomes as liquid biopsy in clinical diagnosis. *Signal Transduct Target Ther.* 2020;5(1):144.
47. Birkhauser FD, Studer UE, Froehlich JM, Triantafyllou M, Bains LJ, Petralia G, et al. Combined ultrasmall superparamagnetic particles of iron oxide-enhanced and diffusion-weighted magnetic resonance imaging facilitates detection of metastases in normal-sized pelvic lymph nodes of patients with bladder and prostate cancer. *Eur Urol.* 2013;64(6):953-60.
48. Yue Y, Wang C, Benedict C, Huang G, Truongcao M, Roy R, et al. Interleukin-10 Deficiency Alters Endothelial Progenitor Cell-Derived Exosome Reparative Effect on Myocardial Repair via Integrin-Linked Kinase Enrichment. *Circ Res.* 2020;126(3):315-29.
49. Atayde VD, Aslan H, Townsend S, Hassani K, Kamhawi S, and Olivier M. Exosome Secretion by the Parasitic Protozoan Leishmania within the Sand Fly Midgut. *Cell Rep.* 2015;13(5):957-67.

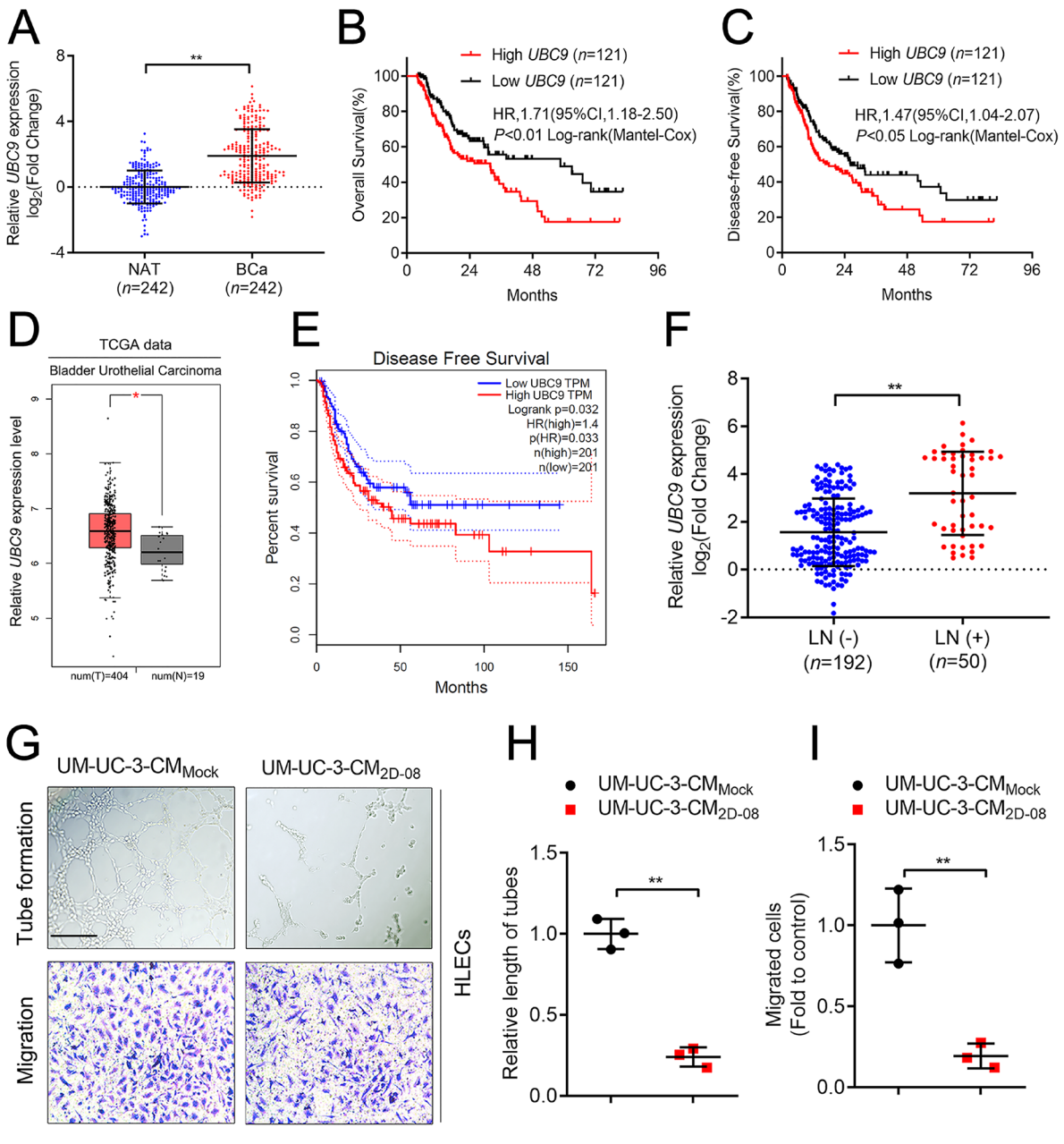

Figure 1. SUMOylation is involved in the LN metastasis of BCa. (**A**) qRT-PCR analysis of SUMOylation core components *UBC9* expression in BCa tissues and paired NATs in a 242-case cohort of BCa patients. The Nonparametric Mann-Whitney *U* test was used to assess the statistical significance. (**B and C**) Kaplan-Meier curves for the OS and DFS of BCa patients with low vs. high *UBC9* expression (cutoff value is the median). (**D**) The expression of *UBC9* in BCa patients compared with controls from TGCA database. (**E**)

Kaplan-Meier survival analysis of BCa patients according to *UBC9* expression from TCGA database (cutoff value is the best cutoff). (**F**) qRT-PCR analysis of *UBC9* expression in LN-positive and LN-negative BCa tissues (n=242). The Nonparametric Mann-Whitney *U* test was used to assess the statistical significance. (**G-I**) Representative images and quantification of tube formation and Transwell migration for HLECs incubation with culture media from indicated UM-UC-3 cells treated with PBS or SUMOylation inhibitor, 2D-08. Scale bars: 100 μm. Two-tailed Student's *t* test was used to assess the statistical significance. Error bars showed the SD of three independent experiments. **P* < 0.05; ***P* < 0.01.

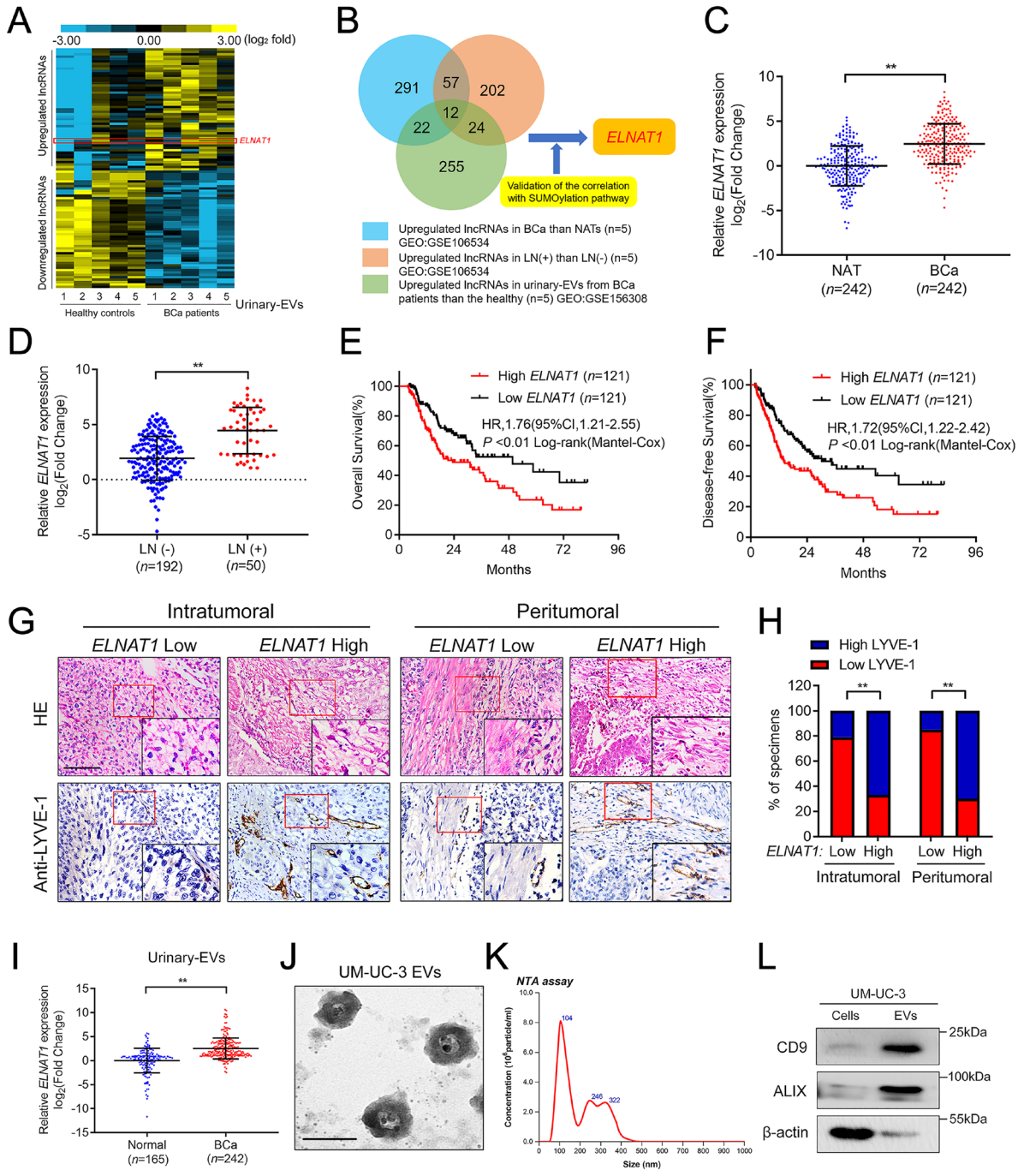

Figure 2. EV-mediated *ELNAT1* overexpression correlates with LN metastasis of BCa. (**A**) Heatmap for the lncRNAs differentially expressed in urinary-EVs from BCa patients and healthy participants. (**B**) Schematic illustrations of the screening of lncRNAs co-upregulated in urinary-EVs from BCa patients and LN-positive BCa tissues. (**C and D**) qRT-PCR analysis of *ELNAT1* expression in BCa tissues and NATs (C), LN-positive and LN-negative

BCa tissues (D) in a 242-case cohort of BCa patients. The Nonparametric Mann-Whitney *U* test was used to assess the statistical significance. (**E and F**) Kaplan-Meier curves for the OS and DFS of BCa patients with low vs. high *ELNAT1* expression (cutoff value is the median). **(G and H)** Representative IHC images and percentages for lymphatic vessel density in BCa tissues according to *ELNAT1* expression. Scale bars: 50 μm. $\chi 2$ test was used to assess the statistical significance. (**I)** qRT-PCR analysis of *ELNAT1* expression in urinary-EVs from 242 BCa patients and 165 healthy participants. The Nonparametric Mann-Whitney *U* test was used to assess the statistical significance. (**J and K**) TEM and NTA identified the characteristics of UM-UC-3-EVs. Scale bars: 100 nm. (**L)** Western blotting analysis of EV markers in cell lysates or UM-UC-3-EVs. Error bars showed the SD of three independent experiments. **P* < 0.05; ***P* < 0.01.

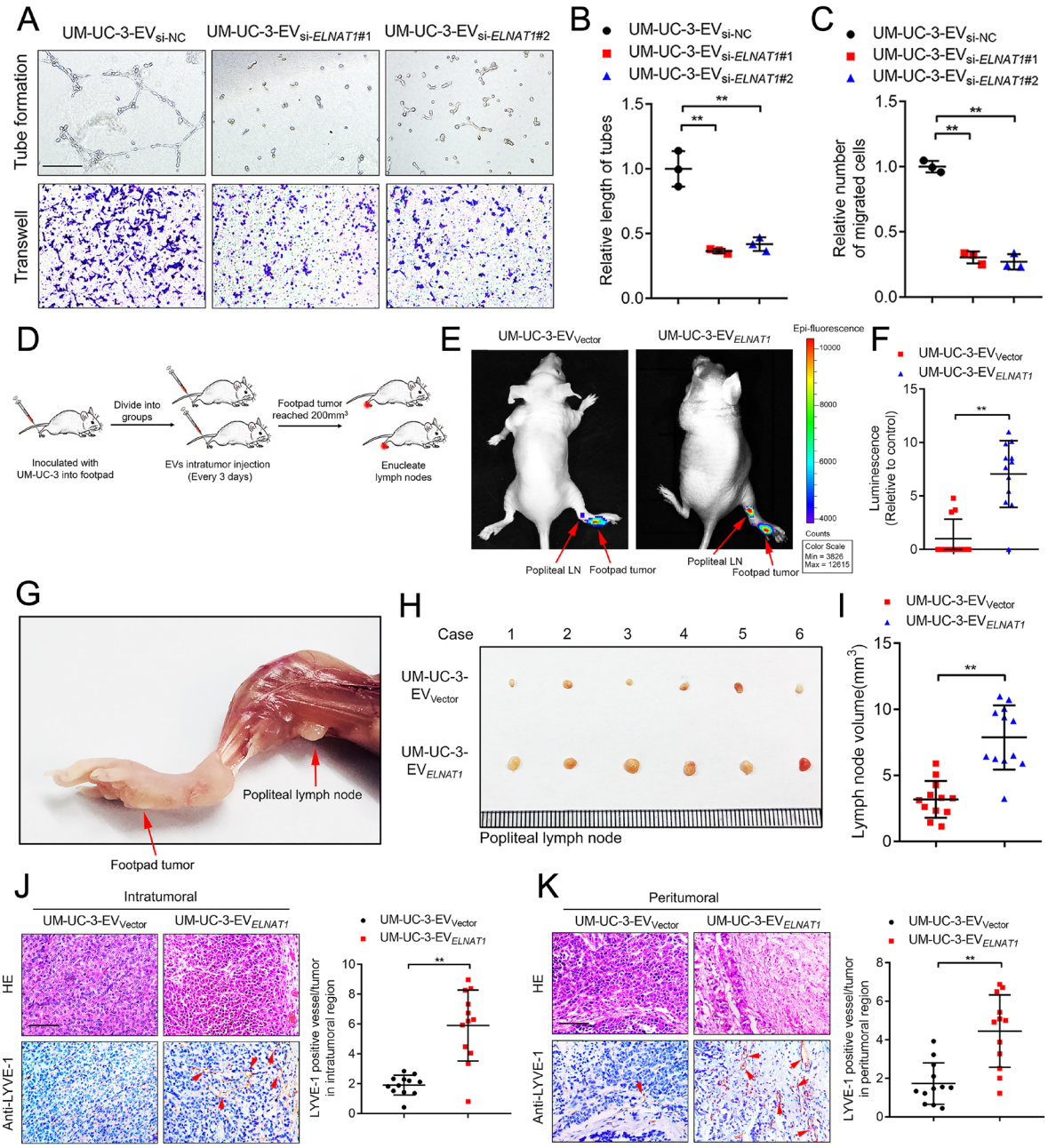

Figure 3. EV-mediated *ELNAT1* facilitates lymphangiogenesis and lymphatic metastasis of BCa in vitro and in vivo. (**A-C**) Representative images and quantification of tube formation and Transwell migration for HLECs treated with UM-UC-3-EV$_{si\text{-}NC}$, UM-UC-3-EV$_{si\text{-}ELNAT1\#1}$ or UM-UC-3-EV$_{si\text{-}ELNAT1\#2}$. Scale bars: 100 μm. 1-way ANOVA followed by Dunnett's tests were used to assess the statistical significance. (**D**) Schematic representation for establishing the nude mouse model of the popliteal LN metastasis. (**E and**

F) Representative bioluminescence images and quantification for the metastatic popliteal LN from nude mice in UM-UC-3-EV_{Vector} or UM-UC-3-EV_{ELNAT1} group (n = 12). The red arrow indicated footpad tumor and metastatic popliteal LN. Two-tailed Student's *t*-test was used to assess the statistical significance. (**G-I**) Representative images and quantification showed the LN volume of UM-UC-3-EV_{Vector} or UM-UC-3-EV_{ELNAT1} group (n = 12). Two-tailed Student's *t*-test was used to assess the statistical significance. (**J and K**) Representative IHC images and quantification of lymphatic vessels in the intratumoral and peritumoral regions of footpad tumors (n = 12). Scale bars: 50 μm. Two-tailed Student's *t*-test was used to detect the statistical significance. Error bars showed the SD of three independent experiments. $*P < 0.05$, $**P < 0.01$.

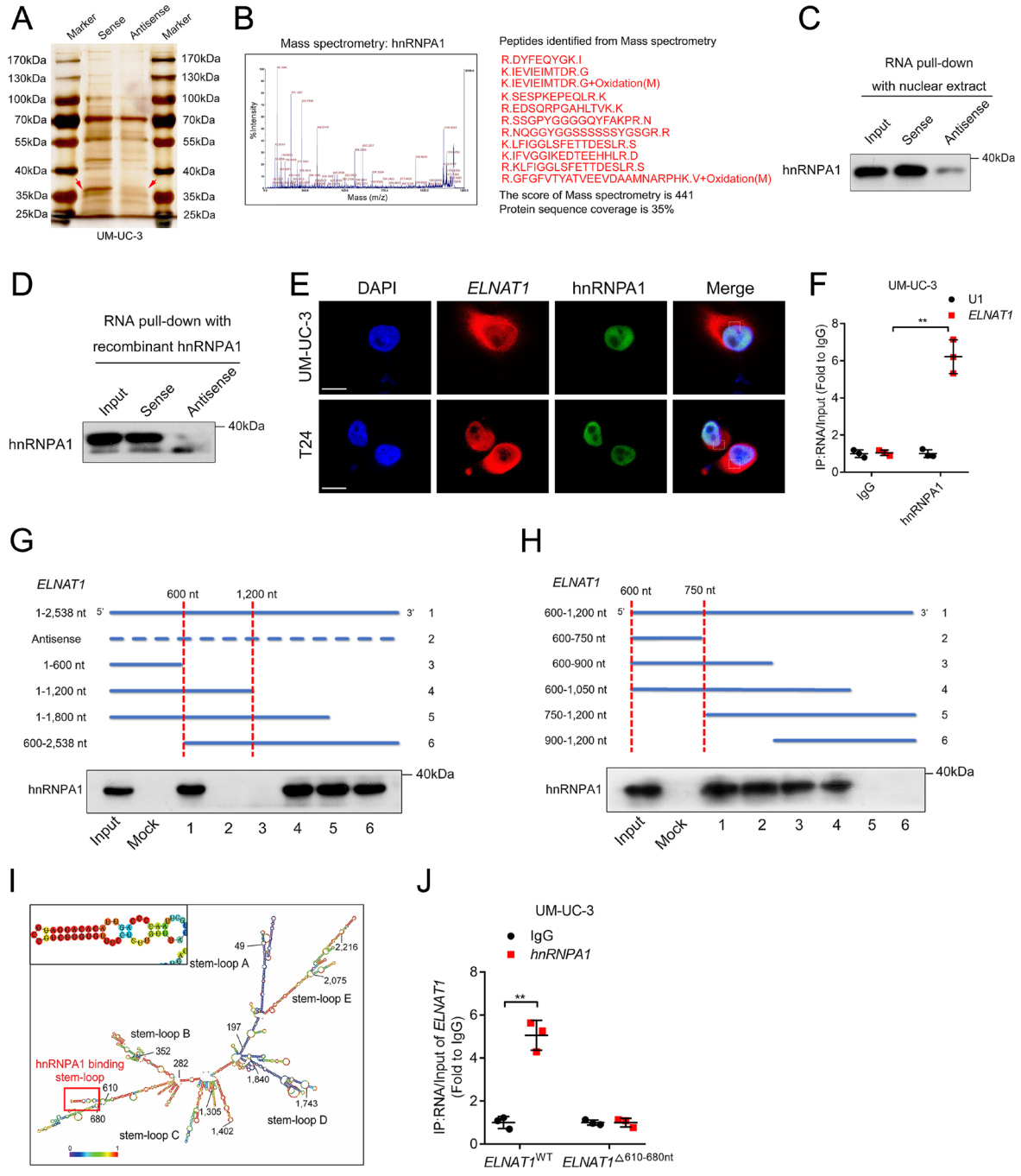

Figure 4. *ELNAT1* directly interacts with hnRNPA1. (**A**) RNA pull-down assay of *ELNAT1* in UM-UC-3 cells. (**B**) Mass spectrometry analysis of the proteins from RNA pull-down assay. (**C and D**) RNA pull-down and western blotting analyses with nuclear extract or purified recombinant hnRNPA1 evaluated the interaction between *ELNAT1* and hnRNPA1. (**E**) Immunofluorescence assessed the colocalization of *ELNAT1* and hnRNPA1

in UM-UC-3 and T24 cells. Scale bar: 5 μm. (**F**) RIP assay using anti-hnRNPA1 assessed the enrichment of *ELNAT1* by hnRNPA1. IgG: negative control; U1: nonspecific control. Two-tailed Student's *t*-test was used to assess the statistical significance. (**G and H**) RNA pull-down assays using serial deletions of *ELNAT1* evaluated the regions required for the binding of *ELNAT1* and hnRNPA1. (**I**) Prediction for the stem-loop structures of hnRNPA1 binding sites in *ELNAT1*. (**J**) RIP assays after the deletion of 610-680-nt of *ELNAT1* in UM-UC-3 cells. Two-tailed Student's *t*-test was used to assess the statistical significance. Error bars showed the SD of three independent experiments. **P* < 0.05, ***P* < 0.01.

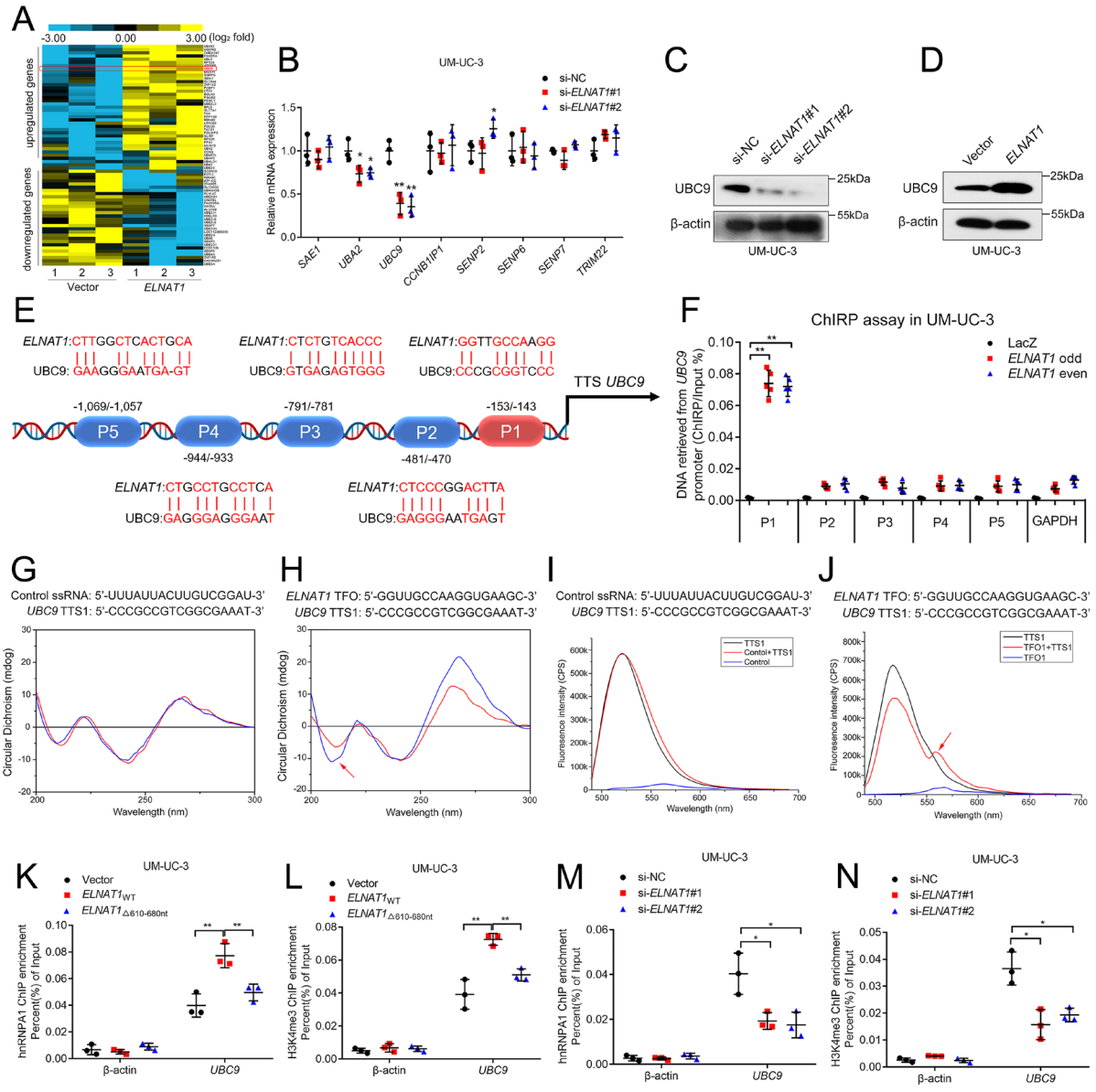

Figure 5. *ELNAT1* forms a DNA-RNA triplex with *UBC9* promoter to enhance H3K4me3 modification by recruiting hnRNPA1. (**A**) Heatmap for the differentially expressed genes after *ELNAT1* overexpressing in indicated BCa cells. (**B**) qRT-PCR analysis of the SUMOylation-related genes after *ELNAT1* knockdown in UM-UC-3 cells. 1-way ANOVA followed by Dunnett's tests were used to assess the statistical significance. (**C and D**) Western blotting analysis of UBC9 expression in UM-UC-3 cells after silencing (C) or overexpressing (D) *ELNAT1*. (**E**) Schematic presentation of the predicted *ELNAT1* binding sites in *UBC9* promoter. **(F)** ChIRP analysis of *ELNAT1*-associated chromatin in UM-UC-3

cells. 1-way ANOVA followed by Dunnett's tests were used to assess the statistical significance. (**G and H**) CD spectrum of TFO in *ELNAT1* with TTS in *UBC9* promoter. The Control ssRNA with TTS in *UBC9* promoter was examined as negative control. (**I and J**) FRET analysis of TFO in *ELNAT1* with TTS in *UBC9* promoter. The Control ssRNA with TTS in *UBC9* promoter was examined as negative control. (**K-N**) ChIP-qPCR analysis of the hnRNPA1 occupancy and H3K4me3 status in *UBC9* promoter in indicated UM-UC-3 cells. 1-way ANOVA followed by Dunnett's tests were used to assess the statistical significance. Error bars showed the SD of three independent experiments. **P* < 0.05, ***P* < 0.01.

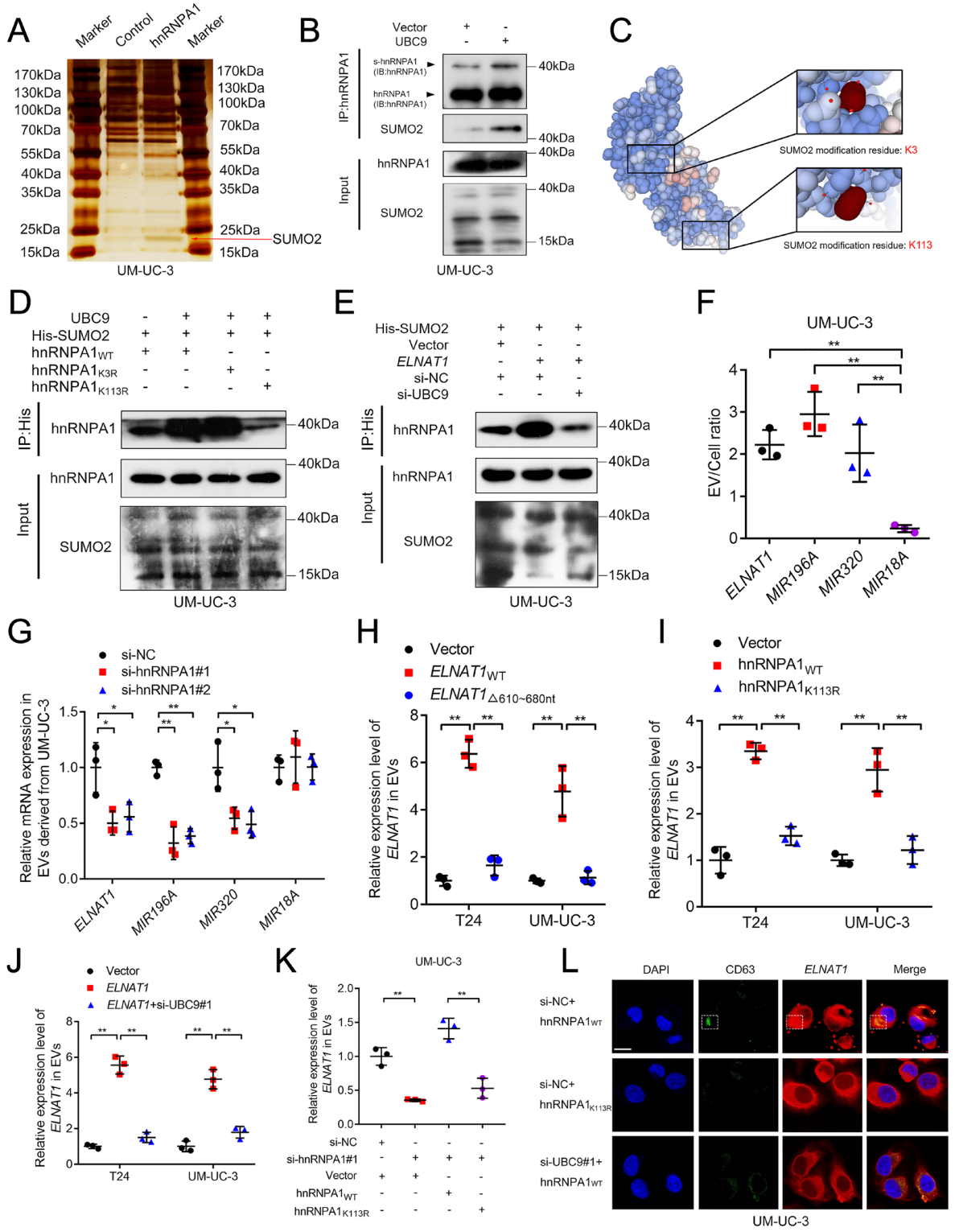

Figure 6. *ELNAT1* is packaged into EVs by UBC9-induced SUMOylation of hnRNPA1. (**A**) co-IP assay using anti-hnRNPA1 in UM-UC-3 cells. Red arrows indicated SUMO2. (**B**) co-IP assay using anti-hnRNPA1 assessed the conjunction of SUMO2 on hnRNPA1 in UM-UC-3 cells after UBC9 overexpressing. (**C**) Schematic representation showed the

predicted SUMO2-conjunct residues on hnRNPA1. (**D**) co-IP assay using anti-His evaluated the conjunction of His-labeled SUMO2 on hnRNPA1 in UM-UC-3 cells after $hnRNPA1_{K3R}$ or $hnRNPA1_{K113R}$ mutation. (**E**) The evaluation of His-labeled SUMO2-conjunction on hnRNPA1 in *ELNAT1*-overexpressing UM-UC-3 cells after UBC9 knockdown by co-IP assay. (**F**) The EV/cell ratio of RNAs in UM-UC-3 cells. (**G**) qRT-PCR analyzed the RNAs expression in EVs secreted by UM-UC-3 cells after hnRNPA1 knockdown. (**H**) The assessment of *ELNAT1* expression in BCa cell-secreted EVs after the deletion of 610-680-nt of *ELNAT1*. (**I**) The analysis of *ELNAT1* expression in BCa cell-secreted EVs after $hnRNPA1_{K113R}$ mutation. (**J**) The evaluation of *ELNAT1* expression in EVs secreted by *ELNAT1*-overexpressing BCa cells after UBC9 knockdown. (**K**) The *ELNAT1* expression in EVs secreted by hnRNPA1-knockdown UM-UC-3 cells after $hnRNPA1_{WT}$ or $hnRNPA1_{k113R}$ overexpression was assessed by qRT-PCR analysis. (**L**) Representative immunofluorescence images showed the accumulation of *ELNAT1* into CD63-indicated MVBs in UM-UC-3 cells after $hnRNPA1_{K113R}$ mutation or UBC9 knockdown. Scale bar: 5 μm. 1-way ANOVA followed by Dunnett's tests were used to assess the statistical significance in **F-K**. Error bars showed the SD of three independent experiments. $*P < 0.05$, $**P < 0.01$.

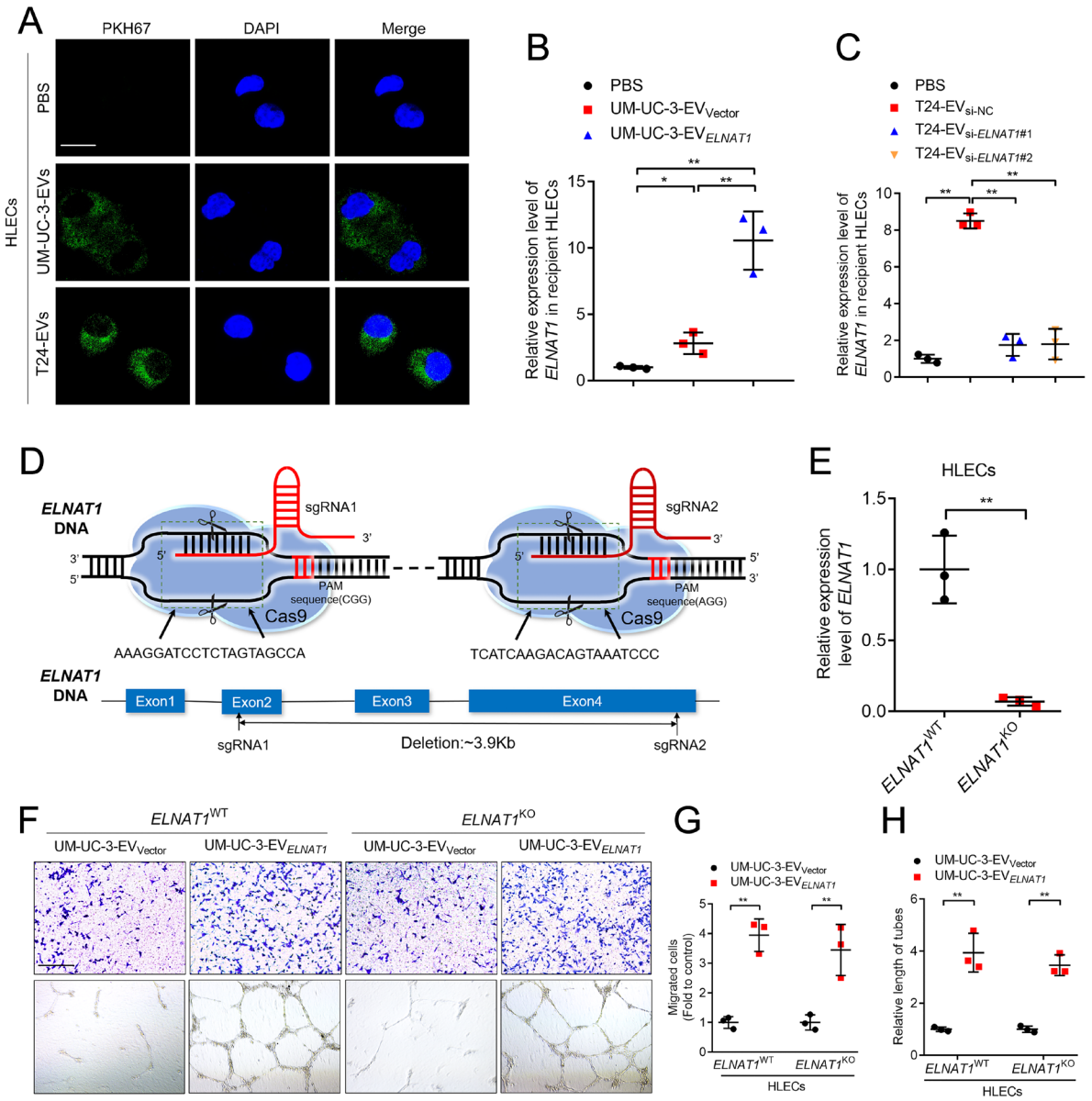

Figure 7. EV-mediated *ELNAT1* is internalized by HLECs to induce lymphangiogenesis. (**A**) Representative immunofluorescence images of PBS or PKH67-labeled (green) EV-treated HLECs. Scale bar: 5 μm. (**B and C**) qRT-PCR analysis of *ELNAT1* expression in HLECs treated with PBS, UM-UC-3-EV$_{Vector}$, UM-UC-3-EV$_{ELNAT1}$ or T24-EV$_{si\text{-}NC}$, T24-EV$_{si\text{-}ELNAT1\#1}$, T24-EV$_{si\text{-}ELNAT1\#2}$. 1-way ANOVA followed by Dunnett's tests were used to assess the statistical significance. (**D**) Schematic illustration of deleting *ELNAT1* in HLECs using the CRISPR/Cas9 approach. (**E**) qRT-PCR analysis validated the successful knockout of *ELNAT1* in HLECs. Two-tailed Student's *t*-test was used to assess the statistical significance. (**F-H**) Representative images and quantification of Transwell migration and tube

formation for *ELNAT1*^{WT} or *ELNAT1*^{KO} HLECs treated with UM-UC-3-EV$_{Vector}$ or UM-UC-3-EV$_{ELNAT1}$. Scale bars: 100 μm. Two-tailed Student's *t*-test was used to assess the statistical significance. Error bars showed the SD of three independent experiments. *$P < 0.05$, **$P < 0.01$.

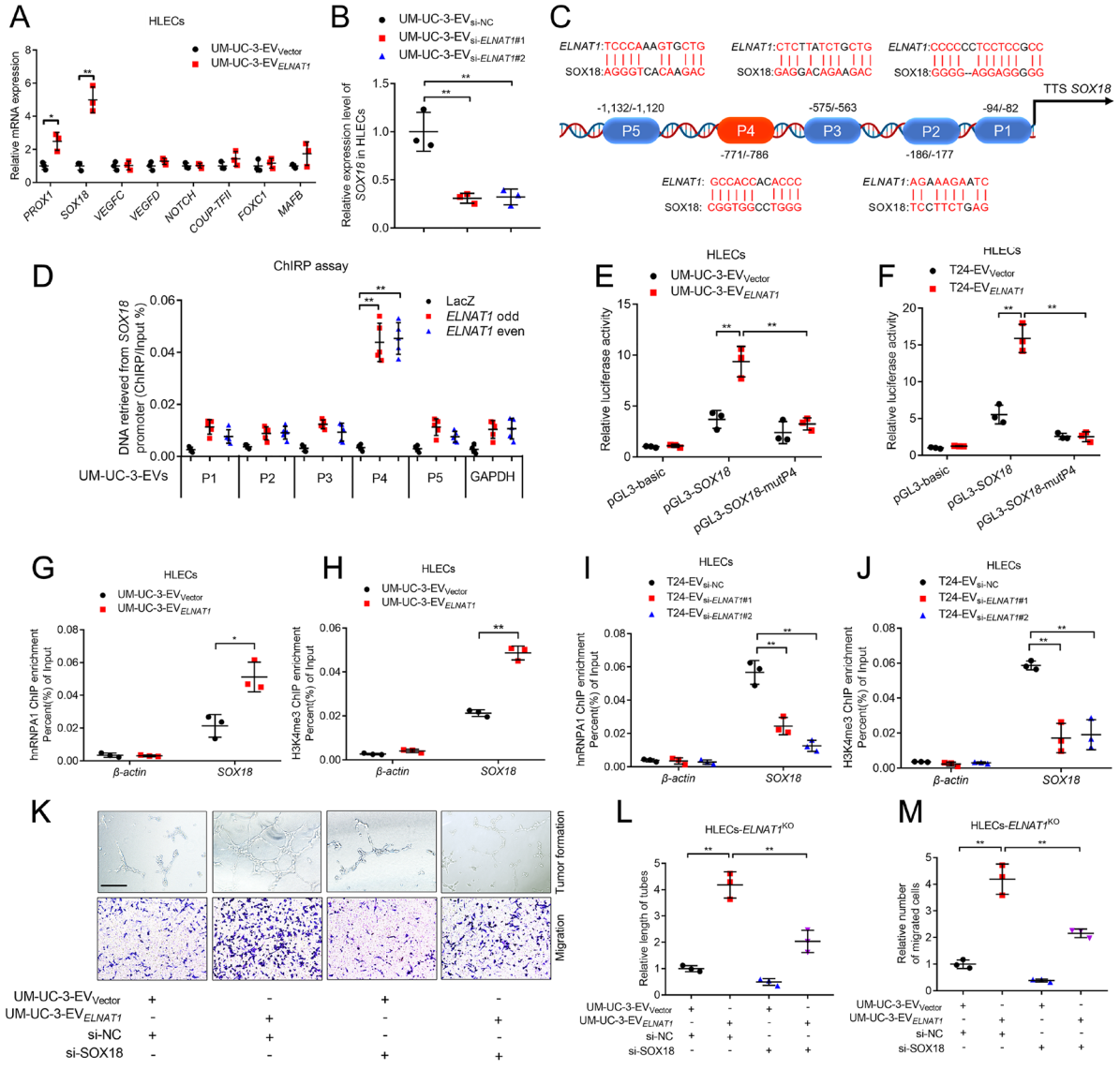

Figure 8. EV-mediated *ELNAT1* upregulates SOX18 expression in HLECs. (**A**) qRT-PCR analysis of lymphangiogenesis-related genes expression in UM-UC-3-EV$_{Vector}$ or UM-UC-3-EV$_{ELNAT1}$-treated HLECs. Two-tailed Student's *t*-test was used to assess the statistical significance. (**B**) qRT-PCR analysis of *SOX18* expression in HLECs treated with UM-UC-3-EV$_{si\text{-}NC}$, UM-UC-3-EV$_{si\text{-}ELNAT1\#1}$ or UM-UC-3-EV$_{si\text{-}ELNAT1\#2}$. 1-way ANOVA followed by Dunnett's tests were used to assess the statistical significance. (**C**) Schematic representation of the predicted EV-mediated *ELNAT1* binding sites in *SOX18* promoter in HLECs. (**D**) ChIRP analysis of EV-mediated *ELNAT1*-associated chromatin in UM-UC-3-EVs-treated HLECs. 1-way ANOVA followed by Dunnett's tests were used to assess the statistical significance. (**E and F**) Luciferase assays for the evaluation of WT or

ELNAT1 binding site mutated *SOX18* promoter in HLECs treated with UM-UC-3-EV_{Vector}, UM-UC-3-EV_{ELNAT1} or T24-EV_{Vector}, T24-EV_{ELNAT1}. 1-way ANOVA followed by Dunnett's tests were used to assess the statistical significance. (**G-J**) ChIP-qPCR analysis of the hnRNPA1 occupancy and H3K4me3 status in the promoter of *SOX18* in HLECs treated with UM-UC-3-EV_{Vector}, UM-UC-3-EV_{ELNAT1} or T24-$EV_{si\text{-}NC}$, T24-$EV_{si\text{-}ELNAT1\#1}$, T24-$EV_{si\text{-}ELNAT1\#2}$. Two-tailed Student's *t*-test or 1-way ANOVA followed by Dunnett's tests were used to assess the statistical significance. (**K-M**) Representative images and quantification of tube formation and Transwell migration for UM-UC-3-EV_{Vector} or UM-UC-3-EV_{ELNAT1}-treated $ELNAT1^{KO}$ HLECs transfected with si-NC or si-SOX18. Scale bars: 100 μm. 1-way ANOVA followed by Dunnett's tests were used to assess the statistical significance. Error bars showed the SD of three independent experiments. $*P < 0.05$, $**P < 0.01$.

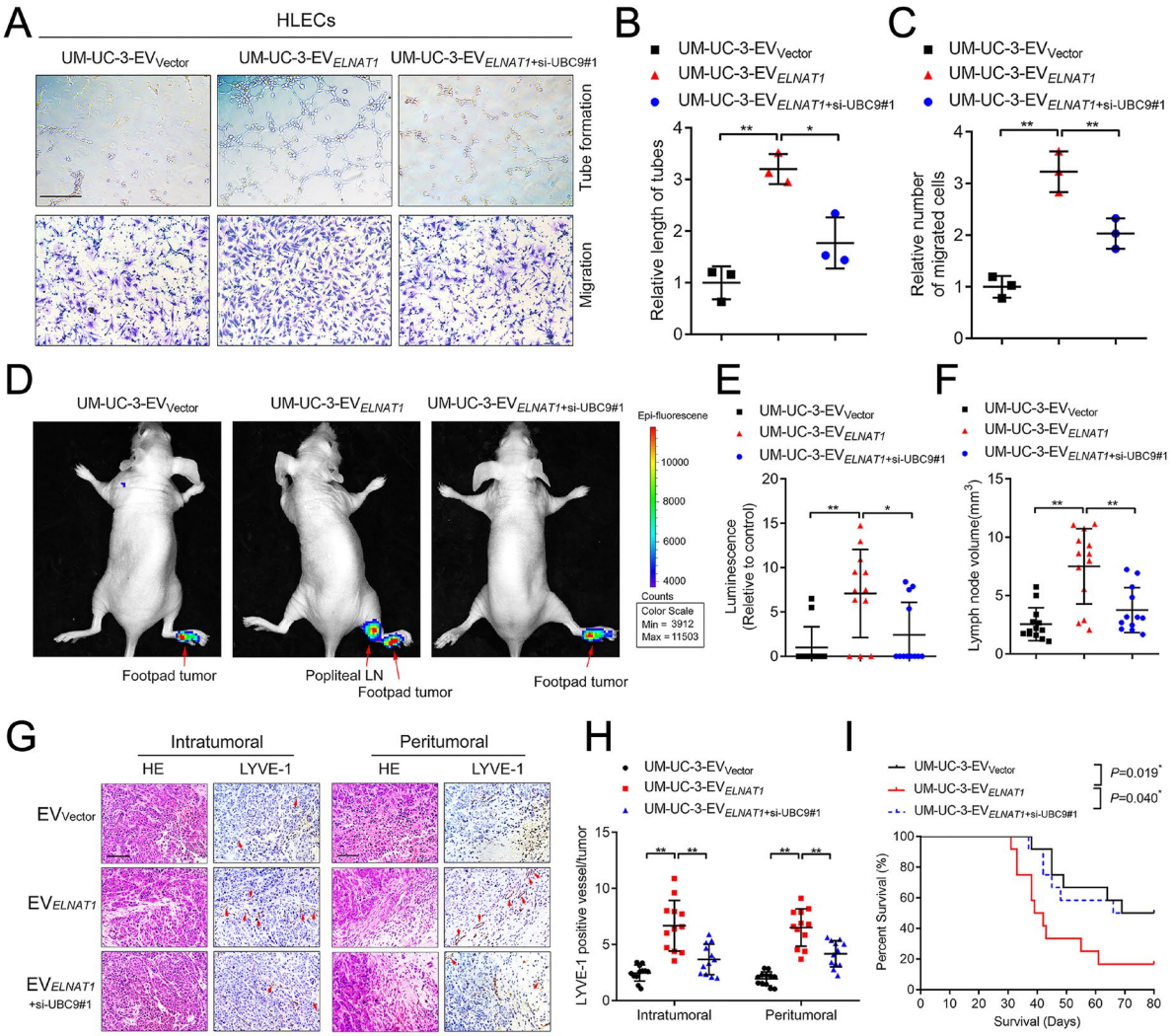

Figure 9. Blocking SUMOylation suppresses EV-mediated *ELNAT1*-induced LN metastasis. (**A-C**) Representative images and quantification of tube formation and Transwell migration for HLECs treated with EVs secreted by control or *ELNAT1*-overexpressing UM-UC-3 cells transfected with si-NC or si-UBC9#1. Scale bars: 100 μm. 1-way ANOVA followed by Dunnett's tests were used to assess the statistical significance. (**D and E**) Representative bioluminescence images and quantification for the popliteal metastatic LN from nude mice treated with EVs secreted by control or *ELNAT1*-overexpressing UM-UC-3 cells transfected with si-NC or si-UBC9#1 (n = 12). The red arrows indicate footpad tumors and metastatic LN. 1-way ANOVA followed by Dunnett's tests were used to assess the

statistical significance. (**F**) Quantification of the popliteal LN volume (n = 12). 1-way ANOVA followed by Dunnett's tests were used to assess the statistical significance. (**G and H**) Representative IHC images and quantification of lymphatic vessels in the footpad tumors (n = 12). Scale bars: 50 μm. 1-way ANOVA followed by Dunnett's tests were used to assess the statistical significance. (**I**) Kaplan-Meier curves showed the survival of nude mice treated with EVs secreted by control or *ELNAT1*-overexpressing UM-UC-3 cells transfected with si-NC or si-UBC9#1. Error bars showed the SD of three independent experiments. *$P < 0.05$, **$P < 0.01$.

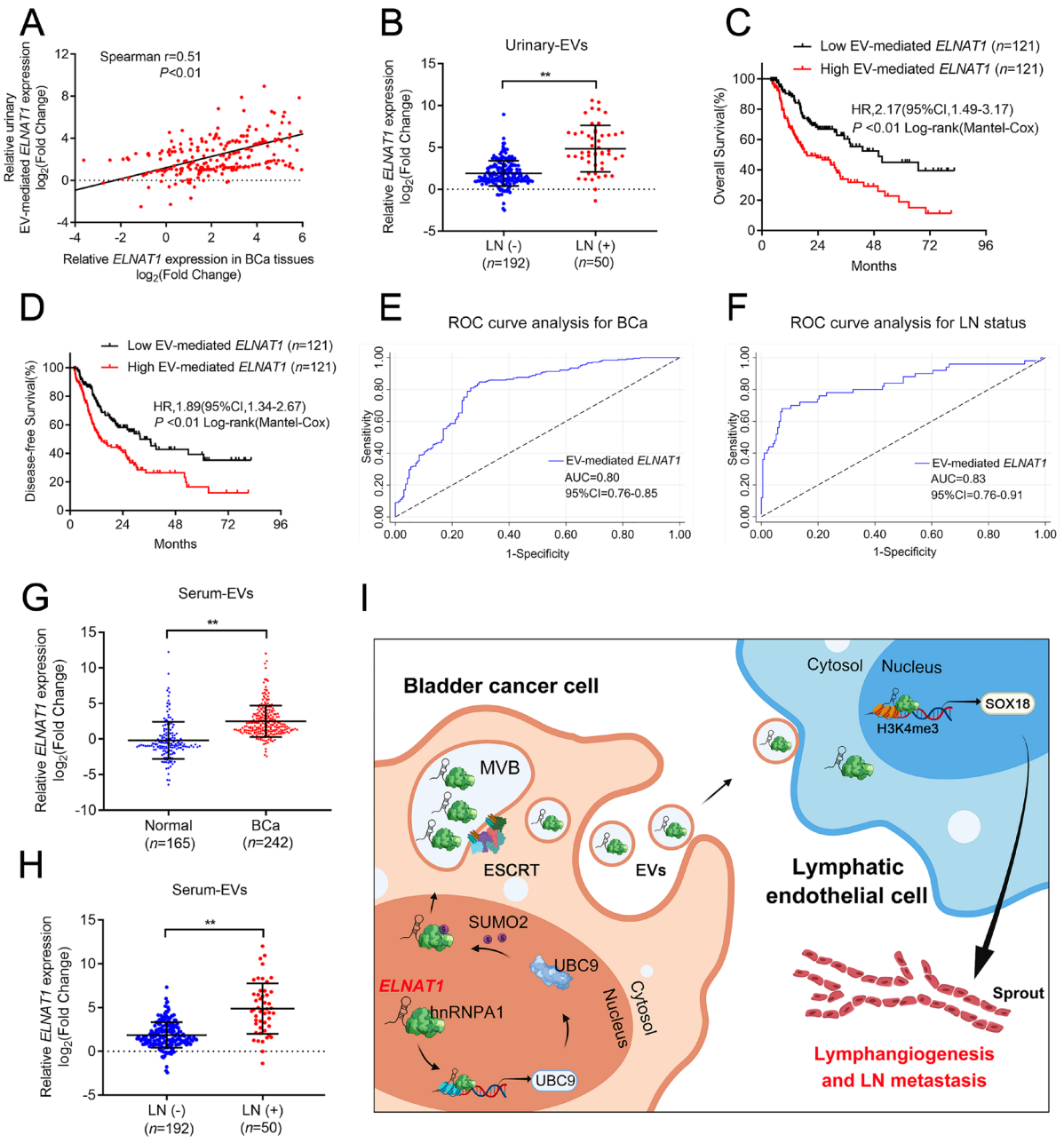

Figure 10. EV-mediated *ELNAT1* is associated with LN metastasis of BCa. (A) Correlation analysis of *ELNAT1* expression in tumor tissues and urinary-EVs from a 242-case cohort of BCa patients. (**B**) qRT-PCR analysis of *ELNAT1* expression in urinary-EVs obtained from a 242-case cohort of BCa patients with or without lymphatic metastasis. The Nonparametric Mann-Whitney *U* test was used to assess the statistical significance. (**C and D**) Kaplan-Meier survival analysis of BCa patients according to EV-mediated *ELNAT1*

expression (cutoff value is the median). (**E and F**) ROC curves for the diagnostic efficiency of urinary EV-mediated *ELNAT1* in diagnosing BCa and LN metastasis. (**G and H**) qRT-PCR analysis of *ELNAT1* expression in serum-EVs obtained from 242 BCa patients and 165 healthy participants (G), LN-positive and LN-negative BCa patients (H). The Nonparametric Mann-Whitney *U* test was used to assess the statistical significance. (**I**) Proposed model of BCa-secreted EV-mediated *ELNAT1* induced the hnRNPA1/UBC9/SOX18 axis to promote lymphangiogenesis and LN metastasis of BCa. Error bars showed the SD of three independent experiments. **P* < 0.05, ***P* < 0.01.